

Dense Discrete Phase Modelling (DDPM) Approach for Hydrodynamics Study of the Gas – Solid Fluidized Bed



By

Malik Qadeer Ahmad

(Registration No: 00000400131)

Department of Chemical Engineering

School of Chemical and Materials Engineering

National University of Sciences & Technology (NUST)

Islamabad, Pakistan

(2024)

Dense Discrete Phase Modelling (DDPM) Approach for Hydrodynamics Study of the Gas – Solid Fluidized Bed



By

Malik Qadeer Ahmad

(Registration No: 00000400131)

A thesis submitted to the National University of Sciences and Technology, Islamabad,
in partial fulfillment of the requirements for the degree of

Master of Science in
Chemical Engineering

Supervisor: Dr. Waheed Miran

Co Supervisor: Dr. Nouman Ahmed

School of Chemical and Materials Engineering
National University of Sciences & Technology (NUST)
Islamabad, Pakistan

(2024)



THESIS ACCEPTANCE CERTIFICATE

Certified that final copy of MS thesis written by Mr Malik Qadeer Ahmad (Registration No 00000400131), of School of Chemical & Materials Engineering (SCME) has been vetted by undersigned, found complete in all respects as per NUST Statues/Regulations, is free of plagiarism, errors, and mistakes and is accepted as partial fulfillment for award of MS degree. It is further certified that necessary amendments as pointed out by GEC members of the scholar have also been incorporated in the said thesis.

Signature: Waheed

Name of Supervisor: Dr Waheed Miran

Date: 25-9-2024

Signature (HOD): [Signature]

Date: 25-09-2024

Signature (Dean/Principal): [Signature]

Date: 26/9/24



National University of Sciences & Technology (NUST)

FORM TH-4

MASTER'S THESIS WORK

We hereby recommend that the dissertation prepared under our supervision by

Regn No & Name: 00000400131 Malik Qadeer Ahmad


Title: Dense Discrete Phase Modeling (DDPM) Approach for Hydrodynamics Study of the Gas-Solid Fluidized Bed.

Presented on: 12 Sep 2024 at: 1430 hrs in SCME Seminar Hall

Be accepted in partial fulfillment of the requirements for the award of Master of Science degree in Chemical Engineering.

Guidance & Examination Committee Members

Name: Dr Muhammad Adnan

Signature: 

Name: Dr Erum Pervaiz

Signature: 

Name: Dr Nouman Ahmad (Co-Supervisor)

Signature: 

Supervisor's Name: Dr Waheed Miran

Signature: 

Dated: 12-09-2024


Head of Department

Date 20-09-2024


Dean/Principal

Date 23/9/24

School of Chemical & Materials Engineering (SCME)

AUTHOR'S DECLARATION

I **Malik Qadeer Ahmad** do hereby state that MS thesis titled “**Dense Discrete Phase Modelling (DDPM) Approach for Hydrodynamics Study of the Gas – Solid Fluidized Bed**” is my own work and has not been submitted previously by me for taking any degree from National University of Sciences and Technology, Islamabad or anywhere else in the country or anywhere in the world.

At any time if my statement is found to be incorrect even after I graduate, the university has the right to withdraw my MS degree.

Name of Student:  **Malik Qadeer Ahmad**

Date: 12 Sep, 2024

PLAGIARISM UNDERTAKING

I solemnly declare that research work presented in the thesis titled “**Dense Discrete Phase Modelling (DDPM) Approach for Hydrodynamics Study of the Gas – Solid Fluidized Bed**” is solely my research work with no significant contribution from any other person. Small contribution/ help wherever taken has been duly acknowledged and that complete thesis has been written by me.

I understand the zero tolerance policy of the HEC and National University of Sciences and Technology (NUST), Islamabad towards plagiarism. Therefore, I as an author of the above titled thesis declare that no portion of my thesis has been plagiarized and any material used as reference is properly referred/cited.

I undertake that if I am found guilty of any formal plagiarism in the above titled thesis even after award of MS degree, the University reserves the rights to withdraw/revoke my MS degree and that HEC and NUST, Islamabad has the right to publish my name on the HEC/University website on which names of students are placed who submitted plagiarized thesis.

Student Signature:  _____

Name: **Malik Qadeer Ahmad** _____

DEDICATION

"This Thesis is dedicated to my PARENTS and FAMILY. I owe all my success to THEM."

ACKNOWLEDGMENT

All praise and eminence are due to "ALLAH," the undisputed architect of this world, who gave us the capacity for comprehension and sparked our curiosity about the planet as a whole. Warmest welcomes to the supreme ruler of this world and the hereafter, "Prophet Mohammed (PBUH)," a source of knowledge and benefits for all of humanity as well as for Umah.

I would like to convey my profound gratitude to **Dr. Waheed Miran, Dr. Nouman Ahmad and Dr. Muhammad Adnan** for their leadership, motivation, helpful suggestions, dedication, and thorough oversight during the project. For their aid during my program, I am appreciative to them. It was a fantastic privilege and an honour to work under their direction. I shall cherish this memory for my entire life.

Additionally, I want to express my gratitude to **Dr. Erum Pervaiz** from the project's advisory group for her informative and helpful suggestions.

TABLE OF CONTENTS

ACKNOWLEDGMENT	VIII
TABLE OF CONTENTS	IX
LIST OF TABLES	XI
LIST OF FIGURES	XII
LIST OF SYMBOLS, ABBREVIATIONS AND ACRONYMS	XIII
ABSTRACT	XIV
CHAPTER 1:	INTRODUCTION
1	
1.1 BACKGROUND	1
1.2 STATEMENT OF PROBLEM	1
1.3 RESEARCH OBJECTIVES AND QUESTIONS.....	1
1.4 SIGNIFICANCE AND MOTIVATION	2
1.5 SCOPE AND LIMITATIONS.....	2
1.6 ORGANIZATION OF THE THESIS.....	2
CHAPTER 2: LITERATURE REVIEW	3
2.1 LITERATURE REVIEW.....	3
CHAPTER 3: THEORETICAL FRAMEWORK	7
3.1 BACKGROUND OF FLUIDIZED BEDS	7
3.2 WORKING PRINCIPLE OF FLUIDIZED BEDS	7
3.3 PARTS OF A FLUIDIZED BED SYSTEM.....	7
3.4 ADVANTAGES OF FLUIDIZED BEDS	8
3.5 DISADVANTAGES AND CHALLENGES	8
3.6 GELDART'S CLASSIFICATION OF POWDER.....	9
3.7 FLUIDIZATION REGIMES	10
3.8 INTRODUCTION TO CFD.....	11
3.9 BASIC CFD APPROACHES FOR MODELLING OF GAS – SOLIDS FLOWS	11
3.10 EULERIAN-EULERIAN APPROACH.....	12
3.11 EULERIAN-LAGRANGIAN APPROACH.....	13
3.12 DISCRETE ELEMENT METHOD (DEM)	14
3.13 DENSE DISCRETE PHASE MODEL (DDPM)	14
3.14 GOVERNING EQUATIONS.....	14
3.14.1 Gas Phase Governing Equations.....	15
3.14.2 Particle Force Balance Equations.....	15
3.15 CLOSURE MODELS FOR GAS AND SOLID PHASE INTERACTIONS	16

3.16 CLOSURE MODELS FOR PARTICLE-PARTICLE INTERACTIONS	16
3.17 DRAG MODELS	18
3.17.1 Gidaspow Model.....	18
3.17.2 Wen-Yu model.....	19
3.18 KINETIC THEORY OF GRANULAR FLOW (KTGF).....	19
CHAPTER 4: METHODOLOGY	20
4.1 INTRODUCTION	20
4.2 MODEL DESCRIPTION	20
4.2.1 Fluidized Bed and Particle Properties	20
4.2.2 Dense Discrete Phase Model (DDPM).....	20
4.3 MESH GENERATION	20
4.3.1 Meshing Strategy	20
4.3.2 Grid Independence Study.....	21
4.4 SIMULATION SETUP	21
4.4.1 Boundary and Operating Conditions.....	21
4.4.2 Solver Settings	21
4.5 COMPARISON WITH EXPERIMENTAL DATA	21
4.5.1 Validation Metrics	21
4.5.2 Interpretation of Results	21
CHAPTER 5: RESULTS AND DISCUSSION	22
5.1 EXPERIMENTAL SETUP.....	22
5.2 SIMULATION SETUP	23
5.2.1 Boundary and Initial Conditions	24
5.3 GRID INDEPENDENCE TEST	26
5.4 COMPARISON BETWEEN GIDASPOW AND WEN – YU DRAG MODEL	29
5.4.1 Instantaneous Solid Volume Fraction Contours.....	29
5.4.2 Time Averaged Axial Profile of Solid Volume Fraction	30
5.4.3 Time Averaged Radial Profile of Solid Volume Fraction	32
5.4.4 Time Averaged Solid Particles Velocity Vector Plot	34
5.5 DRAG MODIFICATION AND DRAG SCALE FACTOR.....	35
5.6 MODIFICATION OF WEN – YU DRAG MODEL	36
5.6.1 Instantaneous Solids Concentration Contours	37
5.6.2 Time Averaged Axial Profile of Solid Volume Fraction	38
5.6.3 Time Averaged Radial Profile of Solid Volume Fraction	40
5.6.1 Time Averaged Solid Particles Velocity Vector Plot	42
CHAPTER 6: CONCLUSION AND RECOMMENDATION	43
REFERENCES	44

LIST OF TABLES

Table 3.1: Characteristics of Geldart Powder [1, 5].....	9
Table 5.1: Solid Particles and Fluidizing Gas Properties [33]	24
Table 5.2: Summary of Boundary Conditions	25
Table 5.3: Summary of Initial Conditions.....	25
Table 5.4: Summary of Solver Settings	25

LIST OF FIGURES

Figure 3.1: Classification of Powders[1]	9
Figure 3.2: Regimes of Fluidization [1].....	10
Figure 3.3: CFD Modelling Approaches	11
Figure 5.1 Simplified Diagram of Experimental Setup by Zhu et al. [2]	22
Figure 5.2: 2D layout of bubbling fluidized bed Zhu et al.[2].....	23
Figure 5.3: Different Mesh Size used for Grid Independence Test	26
Figure 5.4: Instantaneous Solid Volume Fraction Contours.....	27
Figure 5.5: (a) Time Averaged Solid Volume Fraction (b) Axial Profile of Solid Volume Fraction	28
Figure 5.6: (a) Instantaneous Solid Volume Fraction Contour (b) Discrete Solid Volume Fraction contours	29
Figure 5.7: Time Averaged Axial Solid Volume Fraction	30
Figure 5.8: RMSE in Axial Solid Volume Fraction	31
Figure 5.9: Time Averaged Radial Solid Volume Fraction.....	32
Figure 5.10 RMSE in Radial Solid Volume Fraction	33
Figure 5.11: Solid Particles Velocity Vector Plot.....	34
Figure 5.12: (a) Instantaneous Solid Volume Fraction Contours with Correction Factor (C) of 0.3, 0.35, 0.4, 0.5 and 0.6. (b) Discrete Solid Volume Fraction Contours with Correction Factor (C) of 0.3, 0.35, 0.4, 0.5 and 0.6	37
Figure 5.13: Axial Profile of Solid Volume Fraction with different Scale Factors.....	38
Figure 5.14: RMSE in Axial Solid Volume Fraction	39
Figure 5.15: Time Averaged Radial Solid Volume Fraction with different Scale Factors.....	40
Figure 5.16 RMSE Value in Radial Solid Volume Fraction	41
Figure 5.17: Solid Particles Velocity Vector Plot.....	42

LIST OF SYMBOLS, ABBREVIATIONS and ACRONYMS

C_d	Drag coefficient
d_p	Particle diameter (m)
d_{parcel}	Parcel diameter (m)
e_{pp}	Particle-particle restitution coefficient
g	Gravitational acceleration (m/s ²)
H_d	Heterogeneity index
I	Unit tensor
K_{gp}	Interphase momentum exchange coefficient (kg/(m ³ ·s))
$k_{\theta p}$	Diffusion coefficient (kg/(m·s))
m_{parcel}	Mass of parcel (kg)
$m_{particle}$	Mass of particle (kg)
N_p	Number of particles per parcel
N_{parcel}	Number of parcels
p	Gas pressure shared by both the gas and solid phases (Pa)
Re_p	Particle Reynolds number
\mathbf{v}_p	Particle velocity (m/s)
\mathbf{x}_p	Particle position (m)
<i>Greek letters</i>	
ε	(Voidage)
ρ	Density (kg/m ³)
τ	Stress tensor (Pa)
μ	Shear viscosity (kg/(m·s))
λ_p	Bulk viscosity (kg/(m·s))
θ_p	Granular temperature (m ² /s ²)
$\gamma_{\theta p}$	Collisional dissipation of energy (kg/(m·s ³))
<i>Subscripts</i>	
g	Gas phase
p	Solid phase

ABSTRACT

This study focuses on the difficult task of forecasting the hydrodynamics of a bubbling fluidized bed that involves fine Geldart A particles. The existing literature has had limited success in simulating this phenomenon. This study utilized two homogeneous drag models, namely the Wen – Yu drag model and the Gidaspow drag model, coupled with the Dense Discrete Phase Model (DDPM) to predict the hydrodynamics of a bubbling fluidized bed. The DDPM methodology is an innovative discrete phase modeling method that can accurately trace the trajectories of dispersed phase and forecast their size distributions. The simulation findings indicate that both the Wen-Yu and Gidaspow models are inadequate in accurately predicting the solid volume fractions. This is due to the fact that these models do not take into account the cohesive interparticle forces and tend to overestimate the drag force. Nevertheless, the simulation outcomes of the Wen-Yu drag model exhibit superior performance when compared to the Gidaspow model. Thus, the Wen-Yu drag model was corrected by incorporating a scale factor $C=0.35$, resulting in a decrease in the anticipated drag force. This modification led to a notable enhancement in the accuracy of the predicted axial and radial solid concentrations.

Keywords: Gas – Solid Fluidized bed, Homogeneous Drag Models, Hydrodynamics, Dense Discrete Phase Model (DDPM), Two Fluid Model (TFM), Bubbling Bed, Scale Factor

CHAPTER 1: INTRODUCTION

1.1 Background

Fluidized beds reactors are essential to many industrial processes, such as those that produce petro-chemicals, refinery operations, pharmaceuticals, power generation and clean environment. Fluidized bed reactors are commonly utilized because of their superior mass and heat transport properties, which make them appropriate for a variety of uses such as particle coating, combustion, and catalysis [3]. Understanding and predicting the hydrodynamics of gas – solid fluidized beds are critical for optimizing these processes, improving efficiency, and minimizing environmental impacts.

Due to the complexity of fluidized bed systems, research in this field has historically been depended on experimental studies, which may be costly, time-consuming, and difficult to manage [4]. A versatile and affordable substitute for experiments is computational fluid dynamics (CFD) and it has become a potent technique for modelling fluidized bed behavior [5].

1.2 Statement of Problem

Homogeneous drag models like Gidaspow and Wen-Yu are based on empirical correlations and do not accurately capture the complex interactions between Geldart A solid particles and gas medium because these models don't consider the presence of mesoscale structures (bubbles and clusters). This can lead to inaccuracies in predicting pressure drops, particle velocities, and other important parameters in fluidized bed reactors or other processes.

1.3 Research Objectives and Questions

The primary objective of this thesis is to develop a drag model integrated with DDPM approach to predict the hydrodynamics of gas – solid fluidized beds accurately. To achieve this goal, the following specific research questions will be addressed:

1. Which homogeneous drag model among Gidaspow model and Wen-Yu model is better in predicting the gas – solid hydrodynamics?
2. How does the modified drag model differs from homogeneous drag model in predicting the gas – solid hydrodynamics?

1.4 Significance and Motivation

The successful development of a modified drag model can have significant implications for the field of fluidized bed research and industrial applications. This research holds the potential to:

- Increase the precision and effectiveness of fluidized bed hydrodynamics prediction, resulting in more successful process optimization.
- Reduce the need for expensive experimental research, which will save time and money.
- Enable improved understanding and management of fluidized bed systems in diverse industrial operations, hence augmenting environmental performance and sustainability.

1.5 Scope and Limitations

This research will focus on development of modified drag model and its implementation through DDPM approach for predicting gas – solid fluidized bed hydrodynamics. The study will primarily explore the behavior of Geldart A particles in fluidized beds. The limitations of this research include:

- Findings of this study may not be directly transferable to all fluidized bed systems due to variations in particle properties and operating conditions.

1.6 Organization of the Thesis

The remainder of this thesis is organized as follows:

- Chapter 2 includes the literature review on fluidized bed systems and CFD modelling.
- Chapter 3 outlines the theoretical framework, including the fundamental principles of fluidized beds.
- Chapter 4 includes the methodology adopted for carrying out this research work.
- Chapter 5 presents the results and discussions, including the grid independent study, axial and radial profiles based upon different drag models.

CHAPTER 2: LITERATURE REVIEW

2.1 Literature Review

Gas – solid fluidization is a technique utilizing gas to transform a bed of solid particles in a vertical column into a state where they can flow. To counterbalance the gravitational force exerted by the particles, a fluidizing media, such as air, flows through the solid particle bed. Fluidization begins when the upward drag force exerted by the fluidizing medium balances the weight of the solid particles, causing the bed to become suspended. At this stage, the process of fluidization commences and is referred to as the minimal fluidization point [6].

The fluidization process has great worth and it has a very broad application area. Typical application of fluidization process is in fluidized bed reactors [7]. These reactors are used in refineries (for the cracking of valuable low boiling point hydrocarbons from heavy hydrocarbons) [8], the petrochemical industry [9], the pharmaceutical industry, the food industry, and environmental protection. Compared to fixed-bed reactors, fluidized-bed reactors offer many benefits. These include the provision of isothermal conditions due to better mixing of reactants, better transfer of heat and mass, effective solids circulation, and easy loading/unloading of catalysts within the reactor.

Owing the latest developments in computational technology and numerical skills, CFD has become a very strong tool for developing understanding of the intricate flows within a fluidized bed reactor which otherwise may have been very difficult to understand based on experimental results only. The main advantage of the studying the gas – solid fluidized bed with the help of CFD simulation is that it provides an affordable solution for predicting hydrodynamics compared to expensive experiments [10]. Moreover, CFD analysis is a better option compared to experiments that may involve stringent operating conditions (high temperature and pressure), which are expensive, time consuming and pose safety problems.

Complex flow dynamics and the multitude of interactions among solid particles make fluidized bed reactors a challenging numerical modelling problem. For these processes to be as technologically useful as possible, it becomes essential to effectively handle their inherent instability [11-14].

Currently, there are various multiphase modeling methods available for studying the hydrodynamics in fluidized bed reactors. These approaches utilize both commercial [15] and open-source software. Two commonly used numerical techniques for modeling fluidized bed

reactors are the Eulerian-Eulerian two fluid model (TFM) and the Eulerian-Lagrangian discrete phase model (DPM) [16].

The motion of both gas and solid particles is resolved inside an Eulerian frame of reference in TFM. The equations for conservation of mass and momentum are solved independently for each phase. The conservation equations are solved by constitutive models derived from the Kinetic Theory of Granular Flow (KTGF) [17]. Since the TFM approach implies that solids are in a continuum phase, it is necessary to use primarily fine grids for this approach. This approach is employed to investigate the hydrodynamics of small systems, such as those at lab scale or pilot scale, due to this reason [18-24].

In addition, particles are unable to retain their distinct characteristics in the Eulerian-Eulerian approach because they are treated as a continuous phase. As a result, for processes that include multiple particle sizes, extra equations for mass and momentum conservation are necessary for each solid phase [25]. Due to this primary limitation of the Eulerian-Eulerian technique, its use is restricted to small-scale systems consisting of monodisperse particles [26].

Eulerian-Lagrangian approach can be used to overcome the limitations of Eulerian – Eulerian approach because it tracks the individual solid particles or parcel (group of particles having same mass, position, velocity, size and temperature) of particles. In this approach motion of fluid phase is tracked on Eulerian frame of reference and motion of solid particles is resolved using Newton's second law of motion on Lagrangian frame of reference. Discrete element model (DEM) [27], the dense discrete phase model (DDPM) [28-30] and the multiphase particle-in-cell model (MP-PIC) [31, 32] are an example of Eulerian – Lagrangian approach.

The difference between these DPM approaches lies in the method that how these track the solid particles and particle – particle interaction. In DEM individual solid particles are tracked. In DEM individual particles are tracked and where as in DDPM and MP-PIC approach parcels of particles are tracked. In DEM, particle – particle interactions are modelled using detailed collision models (hard sphere or soft sphere approach) whereas collision between particles in DDPM and MP-PIC approach is solved using stochastic collision models are used [33].

DDPM and MP-PIC approaches differ in the method of calculating interparticle collisions. In DDPM collision between particles is tracked based on KTGF [34] and in MP-PIC approach solid stress equation is used for modelling of interparticle collisions [31]. Owing to the benefits of tracking parcels instead of individual particles and using stochastic collision laws, DDPM approach can be used for modelling of industrial scale fluidized bed reactors. However,

research using the DDPM is still in its early stages compared to the Eulerian–Eulerian and DEM approaches, indicating that this model needs more verification and validation.

The powder classification method developed by Geldart categorizes solid particles in fluidized bed systems into four primary groups: Geldart A, B, C, and D. The performance of fluidized bed systems is affected by the properties of the particles, including their size, weight, fines content, and cohesiveness. Geldart A particles have greater fluidization efficiency than Geldart B and D particles due to their smaller size and lower average density [5].

Earlier investigations have employed the aforementioned numerical modeling methods to examine the hydrodynamic characteristics of bubbling fluidized beds containing various types of Geldart particles [35-38]. These experiments have shown that traditional Eulerian-Eulerian and Eulerian-Lagrangian modeling methods are unable to effectively describe complex small-scale formations, such as bubbles or clusters that are smaller than the size of the numerical cells. This limitation is associated with traditional homogeneous drag models, which tend to provide even distributions of solid volume fraction and thus result in increased bed expansion heights [39-43]. The validity of this conclusion is particularly significant for Geldart A particles, as multiple studies have shown that the homogeneous drag model can reliably forecast the hydrodynamics of fluidized beds that contain Geldart B and D particles [17, 44-48].

For Geldart A particles, it has been suggested to use fine grid size to correctly predict the gas – solid hydrodynamics. Lu et al. [49] has shown when the mesh size to particle diameter ratio is 10 then homogeneous drag model coupled with TFM may to be used to resolve the fine structures like bubbles and clusters. Nikolopoulos et al. [50] reported for circulating fluidized bed that grid size to particle diameter ratio of 20 is good enough to produce good numerical results using conventional drag models. Benyahia [51] reported solid volume fraction can be reproduced for circulating fluidized bed if mesh size is 18 times of particle; even in this case value of solid flux predicted was different from the experimental values. It can be concluded that for Geldart A particles there is no consensus about the mesh size selection.

According to van Wachem et al. [52] gravity and drag force are the two most important parameters that have influence in correct prediction of hydrodynamics of fluidized bed and solids stress based on KTGF has minor effect. The poor simulation results for Geldart A particles can be attributed to the substantial cohesive forces between particles, which are

commonly disregarded in the majority of simulations. The majority of CFD computations just consider inter-particle forces that arise from particle collisions. Although cohesive inter-particle forces are thought to be important for fine particles, they are deemed insignificant when dealing with coarse Geldart B particles [53-55].

The presence of strong inter-particle forces results in the aggregation of particles, which in turn increases their effective size. As a result, this minimizes the forces of drag between the fluid and particles, leading to a decrease in the expansion of the bed. The conventional drag models for fluidized beds do not necessarily contain errors when applied to fine particles; they simply overlook the influence of particle agglomeration on the drag between gas and solids [55, 56].

If the cohesive forces have a substantial impact on the fluidization of FCC (Fluid Catalytic Cracking), the task at hand is to formulate precise equations that can effectively represent these forces. The objective is to accurately simulate the inter-particle forces in order to forecast particle agglomeration and its influence on drag force. Regrettably, the method for determining inter-particle van der Waals forces remains an approximation [57].

Mckeen & Pugsley [57] conducted a computational fluid dynamics (CFD) simulation of FCC particles in a bubbling fluidized bed. The researchers employed the two-fluid model (TFM) coupled with a reduced drag force. Inter-particle cohesive forces cause FCC particles to clump together, which reduces the drag force. Hence, it is necessary to decrease the conventional drag force by a factor of 0.2 to 0.3 [57].

This research offers the initial comprehensive validation of a DDPM model that employs the drag reduction technique for a bubbling bed consisting of FCC particles, operating at a superficial gas velocity of 0.06 m/s. To account for the cohesive interactions between particles, which result in an increase in the effective particle diameter, the drag force estimated by the standard Wen-Yu model is reduced by a scaling factor. The simulation results produced using the corrected drag model are being compared with the simulation results obtained using the Wen-Yu Model, Gidaspow drag model, and the experimental results of a bubbling bed of FCC particles [2].

CHAPTER 3: THEORETICAL FRAMEWORK

3.1 Background of Fluidized Beds

The first usage of a fluidized bed reactor in modern times was established in 1922. The reactor utilized in Germany for coal gasification to produce synthesis fuel from coal was a stationary, dense-phase gas – solid fluidized bed reactor. Throughout the last century, there has been significant expansion in the idea of low-velocity "conventional" fluidized bed reactors. Notable advancements involve enhancing the speed of the fluid to generate high-velocity circulating fluidized bed reactors, modifying the substance used to fluidize in order to create liquid-solid and gas-liquid-solid fluidized reactors [1].

3.2 Working Principle of Fluidized Beds

Fluidization is a crucial phenomenon in multiphase flows, occurring when a gas or liquid is forced to pass vertically through a collection of particles at a sufficiently high flow rate. This flow rate ensures that the drag force and buoyancy of the fluid adequately counterbalance the weight of the particles. Subsequently, the particles have the ability to move in relation to one another. During the process of fluidization, the particle bed assumes the visual and functional properties of a real liquid or fluid. Chemical reactors utilizing fluidized beds have distinct benefits such as a substantial interfacial surface area between the fluid and particles, efficient contact between the fluid and particles, effective heat transfer, consistent temperature, and the ability to handle various particle properties and a significant quantity of particulate materials [6, 58-61].

3.3 Parts of a Fluidized Bed System

A typical fluidized bed system consists of the following components:

- **Bed Material:** This is the solid material inside the fluidized bed. It can be catalyst particles in a chemical reactor, sand in a heat exchanger, or any other granular material suitable for the intended process.
- **Fluidizing Medium:** The fluidizing medium can consist of either a gas, such as air or nitrogen, or a liquid, such as water. It goes in from the bottom part of the bed and is responsible for supporting and causing the solid particles to become fluidized.

- **Distributor/Plenum:** The distributor is the structure at the bottom of the fluidized bed that evenly distributes the fluidizing medium across the bed's cross-section. It may consist of nozzles or perforated plates.
- **Gas/Liquid Inlet:** This is the point where the fluidizing medium is introduced into the bed.
- **Outlet:** The outlet allows the fluidizing medium and any products or particles to exit the bed.
- **Heat Exchanger or Reactor:** The fluidized bed reactor or heat exchanger is the main processing unit where chemical reactions, heat transfer, or other processes occur.

3.4 Advantages of Fluidized Beds

- Excellent mixing and uniform temperature distribution.
- High heat and mass transfer rates.
- Enhanced reaction kinetics, making them suitable for catalytic reactions.
- Good control over process parameters.
- Reduced emissions in combustion processes due to lower combustion temperatures.

3.5 Disadvantages and Challenges

- Design and operation can be complex and require careful consideration of parameters like particle size and gas velocity.
- Abrasion and attrition of particles can lead to equipment wear.
- Potential for elutriation (particle entrainment) in high gas velocity conditions.

3.6 Geldart's Classification of Powder

In 1973, Geldart invented a widely recognized system for classifying powders. This system is specifically designed for particles that are fluidized in air under atmospheric circumstances, as shown in Figure 3.1. This categorization categorizes powders into four groups: A, B, C, and D, based on their fluidization tendencies [1, 5].

Table 3.1 provides a comprehensive description of the attributes of these categories. Particles of group C are typically inappropriate for fluidization because they have significant interparticle forces. Groups A, B, and D have a tendency for fluidization and are utilized in various industrial applications such as FCC catalysts, coal gasification, and as catalysts in other chemical reactions [1, 5].

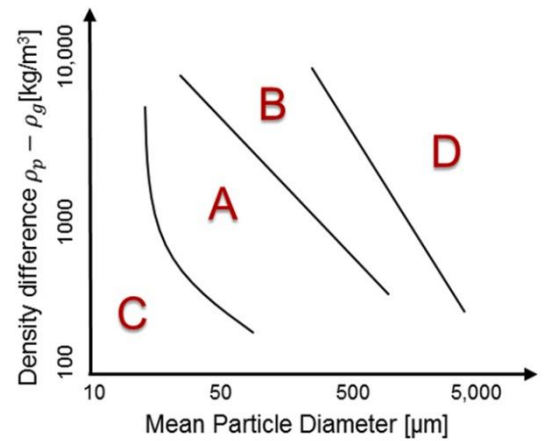


Figure 3.1: Classification of Powders[1]

Table 3.1: Characteristics of Geldart Powder [1, 5]

Group	Example	Salient Feature	Degree of Inter-particle Forces	Particle size range (μm)
C	Starch	Exhibit inadequate fluidization due to strong inter-particle forces, leading to channeling and clumping.	Dominate	<30
A	FCC catalysts, Alumina Powder	Attain the most efficient state of fluidization by using small bubbles; exhibit substantial expansion of the bed and rapid mixing of particles.	Appreciable	~30–100
B	Sand, Glass Beads	Deerate quickly upon cessation of gas flow, resulting in the formation of large bubbles and displaying considerable mixing of solids.	Negligible	~100–800
D	Large Coal Particles	Deerate quickly when gas flow stops; generate large bubbles; exhibit very poor solids mixing in comparison to Geldart B & A type.	Negligible	>800

3.7 Fluidization Regimes

Gas fluidized beds exhibit several distinct flow regimes as the superficial gas velocity increases, as illustrated schematically in Fig. 3.2. As the superficial velocity of gas increases, the bed of particles goes through different flow regimes. It starts with a fixed bed and then transitions to particulate fluidization, which is specific to Group A particles. After that, it progresses to bubbling fluidization, which can turn into slugging in narrow columns. Next, it moves on to turbulent fluidization, fast fluidization, and finally reaches pneumatic transportation [1]. Kwauk et al. [62] based on the type of fluidization behaviors, categorized gas – solid fluidization into two main types: particulate fluidization and aggregative fluidization,

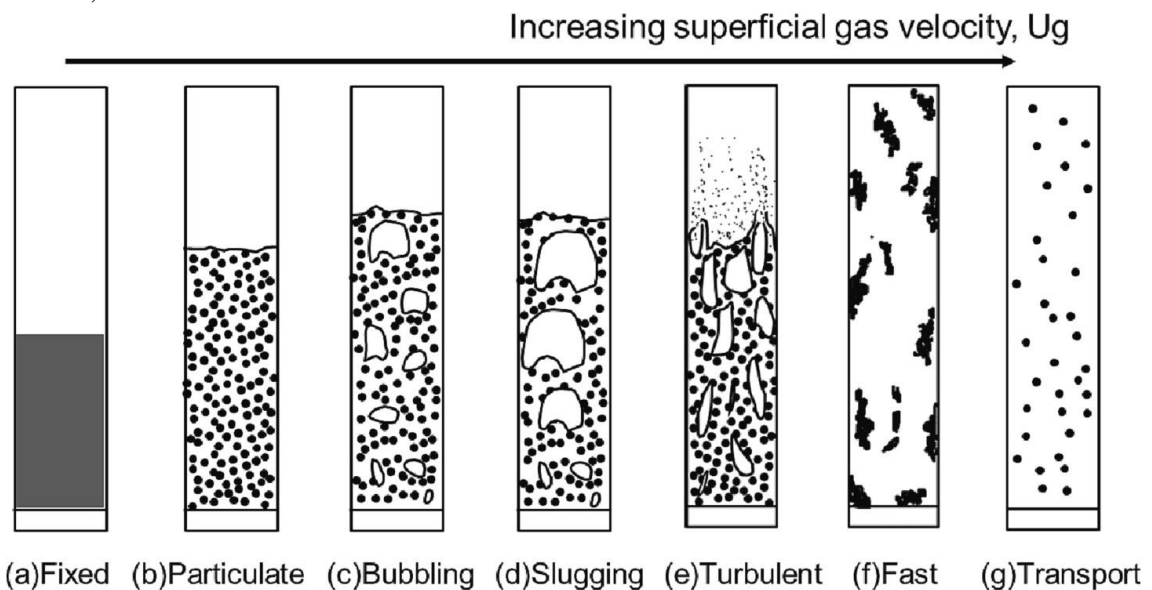


Figure 3.2: Regimes of Fluidization [1]

Figure 3.2(b) is a manifestation of particulate fluidization which is characterized by a homogeneous bed structure where particles are uniformly dispersed and extended throughout the bed. In aggregative fluidization, a fraction of the gas creates separate, discontinuous bubbles that move along the bed, similar to the bubbling fluidization seen in Figure 3.2(c). Bubbles in aggregative fluidization can affect the efficiency of gas-solid contact and influence rates of mass and heat transfer. As a result, they play a crucial role in chemical reactions, especially gas – phase catalytic reactions that rely on interactions between gases and solids [1, 63-65].

3.8 Introduction to CFD

Computational Fluid Dynamics (CFD) is a powerful method used to simulate the movement of fluids and the transfer of heat in gas – solid fluidized beds. This tool enables engineers and researchers to understand the complex interactions between gas and solid particles, which is essential for improving the design and effectiveness of fluidized bed operations. CFD is fundamentally based on the Navier-Stokes equations to accurately represent the behavior of fluids.

Various CFD models are available for predicting gas – solids flows, each with its own set of advantages and drawbacks. The choice of model depends on the user's priorities, such as result accuracy, computational time, and suitability for large-scale systems. Additionally, these models are not yet flawless and have been continually refined over time.

3.9 Basic CFD Approaches for Modelling of Gas – Solids Flows

An overview of different CFD modelling approaches is shown in Figure 3.3. For CFD modelling of gas – solid flows, the Eulerian-Eulerian and Eulerian-Lagrangian methods are the most commonly employed techniques [66]. In the Eulerian-Eulerian approach, both solid and gas phases are treated as being continuous. The Eulerian-Lagrangian approach distinguishes between the fluid phase, which is treated as continuous, and the solid phase, which is treated as discrete.

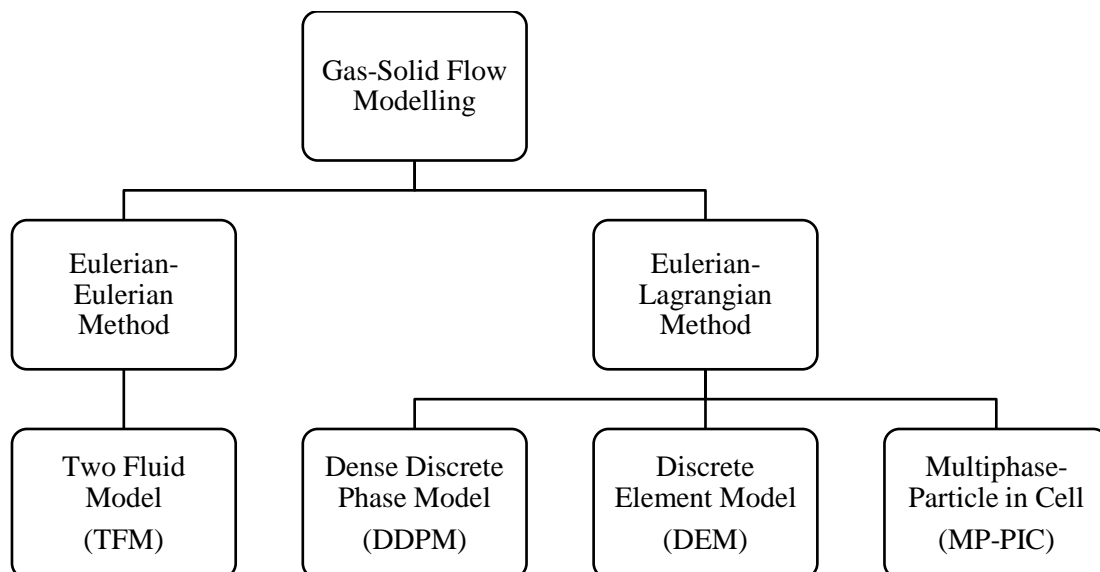


Figure 3.3: CFD Modelling Approaches

The Eulerian-Eulerian model for granular flows is explained using Two Fluid Model (TFM). On the other hand, the Eulerian-Lagrangian approach encompasses three main models: the Dense Discrete Phase Model (DDPM), the Discrete Element Method (DEM), Multiphase-Particle-In-Cell (MP-PIC) method. DEM is based upon tracking the individual solid particles and particle-particle (p-p) interaction is modelled using explicit collision laws like soft sphere model. Both DDPM and MP-PIC models track the parcels (group of particles having same mass, size, position, velocity and temperature). p-p interactions in DDPM are modelled according to KTGF whereas in MP-PIC p-p interactions are represented with simple solid stress equation [33].

3.10 Eulerian-Eulerian approach

In the Eulerian-Eulerian model, the fluid and particles are considered as continuous phases that completely penetrate each other [67]. This implies that the solid phase is represented as a pseudo-fluid [68]. The volume fractions of the phases are seen as continuous functions that vary with both spatial and temporal dimensions. The entire sum of the volume fractions is always equal to one since it is not possible for one phase to occupy the volume of another. The concept is referred to as the phasic volume fraction [69]. The Conservation equations for mass, momentum, and energy for each phase are obtained by employing a suitable averaging technique, commonly known as ensemble averaging [66]. The averaging process produces multiple unresolved terms that require modeling. To tackle this issue, we use constitutive relations that are derived from empirical data or kinetic theory [68].

Two fluid model for gas – solid flows is an example of Eulerian-Eulerian approach. The Eulerian-Eulerian approach typically demands fewer computational resources than the Eulerian-Lagrangian methods. This traditional approach has been crucial in understanding the fluid dynamic properties of gas – solids flow [66]. Nevertheless, this approach has notable constraints when considering fluctuations in particle characteristics, such as variations in particle sizes, diverse densities, and different shapes. The Variations in particle size and density have a significant impact on the flow characteristics of gas – solids systems, such as solid segregation. For these situations, it is necessary to use multiple continuity and momentum equations in order to precisely depict the many types and sizes of particles in this model [31].

However, the cost of including many phases into the computation cannot be disregarded and relies on the computational resources that are accessible. Researchers have observed that the Euler-granular model faces difficulties in accurately representing some properties of real

particles, such as shear stresses and cohesive forces between Geldart A particles when particles are considered as a pseudo-fluid [70].

3.11 Eulerian-Lagrangian Approach

The Eulerian-Lagrangian technique utilizes time-averaged Navier-Stokes equations and extra conservation equations to model the fluid phase. The Handling of the dispersed solid phase involves tracking many particles within the computed flow field. Three-dimensional forces affect the track of each particle, and the computations are performed using Newton's equations of motion [71]. The primary differences among various Eulerian-Lagrangian codes lie in the manner in which particle-particle interactions are handled and the numerical methods utilized to solve the equations [72].

Nevertheless, classic Lagrangian models face substantial constraints when attempting to accurately account for the details of particle-particle and particle-wall collisions [66]. Calculating particle-particle interactions in dense systems with a huge number of particles becomes exceedingly intricate. Simulating such vast systems is impractical, even with supercomputers, due to the substantial computing expense involved in tracking each individual particle [73].

The concept of parcels is employed to reduce the number of particles in computations, significantly speeding up simulations [74]. Garg et al. [75] state that all publicly accessible codes, with the exception of MFiX-DEM, employ a parcel-based methodology for the discrete phase. This method involves monitoring a limited quantity of parcels rather than tracking each individual particle. Each parcel corresponds to a fractional quantity of actual particles, usually combining many particles with comparable characteristics such as the mass, size, position, velocity, and temperature.

These Parcels are alternatively known as computational, numerical, notional, or nominal particles in various literature. ANSYS Fluent has observed that convergence problems may occur when the fluid volume fraction reaches zero. This can happen when the parcel size is larger than the cell size or when too many parcels are compressed into a cell due to the softness of the particles. Increasing the size of parcels decreases the quantity of parcels needed for a specific mass flow, hence reducing computing expenses. Nevertheless, the minimum size of a cell must exceed the maximum size of a parcel. Hence, it is imperative to determine the appropriate equilibrium for the mesh while employing the parcel idea [76].

3.12 Discrete Element Method (DEM)

The soft sphere model, sometimes referred to as the Discrete Element Method (DEM) or Distinct Element Method, is utilized to precisely monitor interactions between particles and between particles and walls in Eulerian-Lagrangian simulations [77]. The model is based on the work of Cundall and Strack. The term often used in literature to describe this strategy is "CFD-DEM." In Discrete Element Method (DEM), collisions or contacts are handled using the numerical integration of the equations of motion represented as a continuous occurrence that takes place over a limited period of time, with the contact force being determined as a continuous function of distance between the particles involved in the collision. This technique is founded on interaction rules that accurately represent physical phenomena, including spring models, spring-dashpot systems, and Coulomb's law of friction [76].

3.13 Dense Discrete Phase Model (DDPM)

The Dense Discrete Phase Model (DDPM) integrated with Kinetic Theory of Granular Flow (KTGF) is a recently developed approach for simulating particle-particle and particle-wall interactions. This model is implemented in both the commercial software ANSYS Fluent and the open-source software OpenFOAM®. It is a hybrid model that combines elements of Eulerian-Eulerian and Eulerian-Lagrangian methodologies. In scenarios with low solids volume fractions, particles are modeled using a Lagrangian approach, while at high solids volume fractions, an Eulerian approach is used. The KTGF provides the stress tensor for calculating the solids stress due to inter-particle interactions, akin to the Euler-granular model for granular flows. Unlike the traditional Lagrangian Discrete Phase Model (DPM), the DDPM-KTGF model is applicable to both dilute and dense phases, as it incorporates the effects of solid phase volume fraction and particle-particle interactions [76].

3.14 Governing Equations

The Dense Discrete Phase Model (DDPM) is a computational approach that uses coarse-grained (CG) technique to monitor and analyze representative particles known as parcels. This approach involves solving the equations for the gas phase in an Eulerian reference frame, while addressing the equations for the solid phase in a Lagrangian reference frame. The names "Hybrid Eulerian-Lagrangian approach," "CG-DDPM approach," and "DDPM approach" are synonymous in the literature [78].

3.14.1 Gas Phase Governing Equations

Continuity equation:

$$\frac{\partial(\varepsilon_g \rho_g)}{\partial t} + \nabla \cdot (\varepsilon_g \rho_g \mathbf{v}_g) = 0 \quad (1)$$

Momentum balance equation:

$$\frac{\partial(\varepsilon_g \rho_g \mathbf{v}_g)}{\partial t} + \nabla \cdot (\varepsilon_g \rho_g \mathbf{v}_g \mathbf{v}_g) = -\varepsilon_g \nabla p + \nabla \cdot \tau_g + \varepsilon_g \rho_g \mathbf{g} + K_{DPM}(\mathbf{v}_p - \mathbf{v}_g) \quad (2)$$

where ε_g denotes the gas phase voidage, ρ_g stands for the gas phase density, \mathbf{v}_g represents the gas phase velocity, \mathbf{v}_p indicates the solid phase velocity, τ_g is the gas phase stress tensor, \mathbf{g} symbolizes the gravitational acceleration, and K_{DPM} is the interphase momentum exchange coefficient between the gas and solid phases [79, 80]. Meanwhile, the term K_{DPM} (drag only) is calculated by determining the solid volume percentage within a numerical cell using the Eulerian method, taking into account only the drag impact.

3.14.2 Particle Force Balance Equations

$$\frac{dv_p}{dt} = F_D(\mathbf{v}_g - \mathbf{v}_p) + \frac{\mathbf{g}(\rho_p - \rho_g)}{\rho_p} - \frac{\nabla p}{\rho_p} - \frac{\nabla \tau_p}{\rho_p} \quad (3)$$

Where v_p denotes the particle phase velocity, μ is viscosity, C_d is drag coefficient, Re is particle Reynolds number, ρ_p is particle density, d_p is particle diameter, ∇p is pressure term, $\nabla \tau_p$ is particle phase stress tensor, \mathbf{g} is gravitational acceleration.

$$\frac{dx_p}{dt} = v_p \quad (4)$$

\mathbf{v}_p is particle velocity and x_p is particle position.

Solid phase volume fraction is as under:

$$\varepsilon_p = \frac{n_{parcel} n_p V_p}{V_{cell}} \quad (5)$$

Gas phase volume fraction is as under:

$$\varepsilon_g = 1 - \varepsilon_p \quad (6)$$

3.15 Closure Models For Gas And Solid Phase Interactions

In order to fully account for mass conservation, momentum conservation, and particle force balancing, it is crucial to incorporate closure factors that consider the interactions between the gas and solid phases, as well as the interactions between the solid particles. [78]. The CG-DDPM model incorporates the drag force term to account for the interaction between the phases:

$$F_D = K_{DPM}(v_p - v_g) \quad (7)$$

K_{DPM} is calculated by adding up the drag forces applied to every solid particle within each computing cell.

$$K_{DPM}(v_p - v_g) = \sum_{i=1}^N \frac{m_i F_D(v_g - v_{pi})}{V_{cell}} \quad (8)$$

In this equation, m_i is the mass of particle i , v_{pi} represents the velocity of particle i , $F_D(v_g - v_{pi})$ is the acceleration caused by drag force per unit particle mass, and V_{cell} is the volume of a cell. The calculation of K_{DPM} depends on the drag model.

Eq. (8) gives the physical meaning of K_{DPM} in respect of the CG-DDPM approach. The drag force (F_D) in Eq. (8) can be defined as follows:

$$F_D = \frac{18\mu C_d Re_p}{24\rho_p d_p^2} \quad (9)$$

3.16 Closure Models For Particle-Particle Interactions

The CG-DDPM approach incorporates interactions between particles through the solids stress tensor (τ_p) in the Eulerian reference frame. This tensor is obtained through the application of the Kinetic Theory of Granular Flow (KTGF) [78].

$$\tau_p = -p_p I + \varepsilon_p \mu_p (\nabla V_p + \nabla V_p^T) + \varepsilon_p \left(\lambda_p - \frac{2}{3} \mu_p \right) \nabla \cdot V_p I \quad (10)$$

The solids stress tensor (τ_p) encompasses both shear viscosity (μ_p) and bulk viscosity (λ_p), which result from the exchange of particle momentum during translation and collisions.

The shear viscosity (μ_p) is defined as under:

$$\mu_p = \mu_{p,kin} + \mu_{p,col} + \mu_{p,fr} \quad (11)$$

Where $\mu_{p,col}$ is collision term, $\mu_{p,kin}$ is kinetic term and $\mu_{p,fr}$ is frictional term. Shear viscosity μ_p is sum of these three terms.

Kinetic viscosity $\mu_{p,kin}$ is defined as under [81]:

$$\mu_{p,kin} = \frac{10}{96} \sqrt{\Theta\pi} \frac{\rho_s d_s}{(1 + e_s) \alpha_s g_0} \left[1 + \frac{4}{5} g_0 \alpha_s (1 + e_s) \right]^2 \quad (12)$$

Collisional viscosity $\mu_{p,col}$ is defined as under [81]:

$$\mu_{p,col} = \frac{4}{5} \varepsilon_p \rho_p d_p g_0 (1 + e_{pp}) \sqrt{\frac{\theta_p}{\pi}} \quad (13)$$

Frictional viscosity $\mu_{p,fr}$ is defined as under [82]

$$\mu_{p,fr} = \frac{P_p \sin \phi}{2\sqrt{l_{2D}}} \quad (14)$$

The bulk viscosity of solids (λ_p) represents the resistance of granular particles to compression and expansion. This concept is modeled according to the work of Lun et al.[83].

$$\lambda_p = \frac{3}{4} \varepsilon_p \rho_p d_p g_0 (1 + e_{pp}) \sqrt{\frac{\theta_p}{\pi}} \quad (15)$$

The solids pressure (p_p) consists of both kinetic and particle collision components. Lun et al. [83] provided a model for it.

$$p_p = \varepsilon_p \rho_p \theta_p + 2\rho_p (1 + e_{pp}) \varepsilon_p^2 g_0 \theta_p \quad (16)$$

The radial distribution function (g_o) serves as a correction factor that adjusts the collision probability between grains as the particle phase becomes dense. Lun et al. [83] proposed a model for this function in the case of a monodisperse particle phase.

$$g_o = \frac{1}{\left[1 - \sqrt[3]{\frac{\varepsilon_p}{\varepsilon_{p,max}}} \right]} \quad (17)$$

The granular temperature (θ_p), which signifies the kinetic energy of the fluctuating particles, can be obtained from the Kinetic Theory of Granular Flow (KTGF) through the following derivation.

$$\frac{3}{2} \left[\frac{\partial}{\partial t} (\rho_p \varepsilon_p \theta_p) + \nabla \cdot (\rho_p \varepsilon_p \theta_p \mathbf{v}_p) \right] = \nabla v_p : (-p_p I + \tau_p) + \nabla \cdot (k_{\theta_p} \nabla \theta_p) - \gamma_{\theta_p} + \phi_{gp} \quad (18)$$

Disregarding the convective and diffusive terms in the equation mentioned above results in following algebraic expression:

$$0 = (-p_p I + \tau_p) : \nabla v_p - \gamma_{\theta_p} + \phi_{gp} \quad (19)$$

Prior Research on the CG-DDPM method has demonstrated that employing the algebraic formulation of the granular temperature produces precise outcomes when simulating bubbling fluidized beds. [26, 33, 78, 80, 84]. Therefore, in this study, we utilized an algebraic method to solve the granular temperature equation. The collisional dissipation of energy ($\gamma\theta_p$) in Eq. (19) is modeled by Lun et al.[83].

$$\gamma\theta_p = \frac{12(1 - e_{pp}^2)g_o}{d_p\sqrt{\pi}}\rho_p\varepsilon_p^2\theta_p^{\frac{3}{2}} \quad (20)$$

The energy exchange between fluid and solid particles (ϕ_{gp}) is represented by the following equation:

$$\phi_{gp} = -3\beta_{gp}\theta_p \quad (21)$$

3.17 Drag Models

In fluidized bed simulations within the realm of CFD, it's crucial to understand how particles interact and how momentum transfers between different phases. Specifically, the interaction between particles and the continuous gas phase is described by drag models, which have been developed for this specific purpose. These models accurately capture the momentum exchange between phases, with drag being a key term in the momentum equation for the granular phase. The choice of drag models significantly impacts the dynamics of the granular phase, leading to noticeable effects on predicted bed expansion and particle concentration in densely populated regions of the bed. The following section outlines the equations central to the drag models used in this study.

3.17.1 Gidaspow Model

Gidaspow model is a combination of the Ergun equation and Wen-Yu model [33, 85]. According to this drag model, when gas volume fraction is less than or equal to 0.8, then Ergun equation is used for calculation of momentum exchange coefficient and for dilute systems having gas volume fraction more than 0.8, Wen – Yu model is used for said calculation.

The Ergun equation integrates aspects of both the Kozeny Carman equation and the Burke Plummer equation [86]. The Kozeny Carman equation forms the first part of the Ergun equation, addressing the viscous flow regime characterized by low Reynolds numbers. The second part, represented by the Burke Plummer equation, pertains to the kinetic flow regime typical of high Reynolds numbers [87].

The interphase momentum exchange coefficient, K_{gp} in this drag model is defined as follows:

Ergun equation:

$$K_{gp-Ergun} = 150 \frac{\varepsilon_p(1 - \varepsilon_g)\mu_g}{\varepsilon_g d_p^2} + 1.75 \frac{\rho_g |\mathbf{v}_p - \mathbf{v}_g|}{d_p}, \varepsilon_g \leq 0.80 \quad (22)$$

Wen-Yu model:

$$K_{gp-WenYu} = \frac{3}{4} C_d \frac{\varepsilon_p \varepsilon_g \rho_g |\mathbf{v}_p - \mathbf{v}_g|}{d_p} \varepsilon_g^{-2.65}, \varepsilon_g > 0.80 \quad (23)$$

where, $|\mathbf{v}_p - \mathbf{v}_g|$ is the slip velocity and C_d is the drag coefficient. The drag coefficient C_d can be defined as follows:

$$C_d = \frac{24}{\varepsilon_g Re_p} \left[1 + 0.15(\varepsilon_g Re_p)^{0.687} \right], Re_p < 1000 \quad (24)$$

$$C_d = 0.44, Re_p \geq 1000 \quad (25)$$

3.17.2 Wen-Yu model

The interphase momentum exchange coefficient, K_{gp} in the Wen-Yu model is defined as follows [33]:

$$K_{gp-WenYu} = \frac{3}{4} C_d \frac{\varepsilon_p \varepsilon_g \rho_g |\mathbf{v}_p - \mathbf{v}_g|}{d_p} \varepsilon_g^{-2.65} \quad (23)$$

where C_d is the drag coefficient which can be defined as follows:

$$C_d = \frac{24}{\varepsilon_g Re_p} \left[1 + 0.15(\varepsilon_g Re_p)^{0.687} \right] \quad (24)$$

$$C_d = 0.44, Re_p \geq 1000 \quad (25)$$

3.18 Kinetic Theory of Granular flow (KTGF)

The kinetic theory of granular flow explains how groups of large particles like sand or powders behave. Unlike gases, where particles flow continuously, granular materials behave in a more distinct, collision-focused way. This theory examines how these particles interact, collide, and exchange energy. Granular flows show interesting behaviors such as segregation and clustering, which challenge traditional fluid dynamics methods. Understanding granular dynamics is crucial in various industries like agriculture and pharmaceuticals, as well as in natural events like landslides. The kinetic theory of granular flow helps predict and manage these materials' behavior, leading to advancements in handling and processing granular substances across different fields [17].

CHAPTER 4: METHODOLOGY

4.1 Introduction

This chapter presents the methodology employed in the computational fluid dynamics (CFD) modelling of a bubbling fluidized bed (BFB) specifically for Geldart A particles using the Discrete Phase Particle Model (DPPM). The chapter outlines the procedures followed for mesh generation, simulation setup, and the comparison of simulation results with experimental data.

The primary objective of this research is to simulate the behavior of Geldart A particles in a bubbling fluidized bed using CFD. Specifically, the axial, radial, and solid volume fraction profiles obtained from the simulations will be compared with experimental data. This comparison aims to validate the accuracy of the CFD model and assess its predictive capabilities in simulating Geldart A particle behavior in a fluidized bed.

4.2 Model Description

4.2.1 Fluidized Bed and Particle Properties

The fluidized bed geometry and operating conditions were based on experimental data Zhu et al. [2]. Geldart A particles, characterized by their behavior in fluidization regimes, were selected for the simulations. The physical and flow properties of both the particles and the gas phase were defined to accurately represent the experimental setup.

4.2.2 Dense Discrete Phase Model (DDPM)

DDPM was employed to simulate the behavior of Geldart A particles in the fluidized bed. This model tracks the motion of individual particles by solving the equations of motion for a parcel of particles in the Lagrangian framework. The interphase interactions between particles and the fluid were accounted for using modified Wen-Yu drag model with the help of UDF.

4.3 Mesh Generation

4.3.1 Meshing Strategy

The computational domain was discretized using a structured mesh generated in Gambit 2.4.6. The mesh was designed to capture the complex flow dynamics within the fluidized bed, ensuring sufficient resolution near the walls and areas of interest such as the bubble region.

4.3.2 Grid Independence Study

To ensure the accuracy and reliability of the results, a grid independence study was conducted based on three squared mesh sizes (4mm, 5mm and 7mm). Mesh refinement was performed iteratively until the changes in the simulation results became negligible, indicating grid-independent solutions for the desired parameters.

4.4 Simulation Setup

4.4.1 Boundary and Operating Conditions

The boundary conditions were set based on the experimental setup [2], including inlet velocities, particle properties, and initial conditions. The gas-solid flow within the fluidized bed was simulated 21 s, it included 1 s for injection of particles, next first 10 s simulation was based on transient conditions and remaining 10 s simulation was carried out on data statistics.

4.4.2 Solver Settings

The simulations were performed using a commercial CFD software package (Ansys Fluent R21) capable of solving multiphase flow problems. The discretized governing equations for fluid flow and particle motion were solved numerically using appropriate solvers and algorithms to ensure accurate predictions of particle behavior in the fluidized bed.

4.5 Comparison with Experimental Data

4.5.1 Validation Metrics

The axial, radial, and solid volume fraction profiles obtained from the simulations were compared with experimental data available [2]. Quantitative metrics such as root mean square error (RMSE) was used to assess the agreement between simulation results and experimental measurements.

4.5.2 Interpretation of Results

The comparison between simulation and experimental data provided insights into the accuracy and predictive capabilities of the CFD model. Discrepancies between simulation and experimental results were analyzed to identify potential areas for model improvement and to validate the assumptions and simplifications made in the CFD model.

CHAPTER 5: RESULTS AND DISCUSSION

5.1 Experimental Setup

Experimental data has been taken for validation from the work of Zhu et al. [2] shown in Fig 5.1. In this experiment, column made of Plexiglas having internal diameter of 0.267m has been used. The height of fluidizing column is 2.464m. Air has been as fluidizing medium and it has been fed through perforated distributor pipe made of aluminum. Air flowrate has been measured with the help of orifice plate. Gas velocity of 0.06 m/s has been used for fluidizing the bed of particles. Solid particles used are Geldart A particles resembling FCC catalyst particles having mean particle diameter of 51.8 micron and density of 1780 kg/m³.

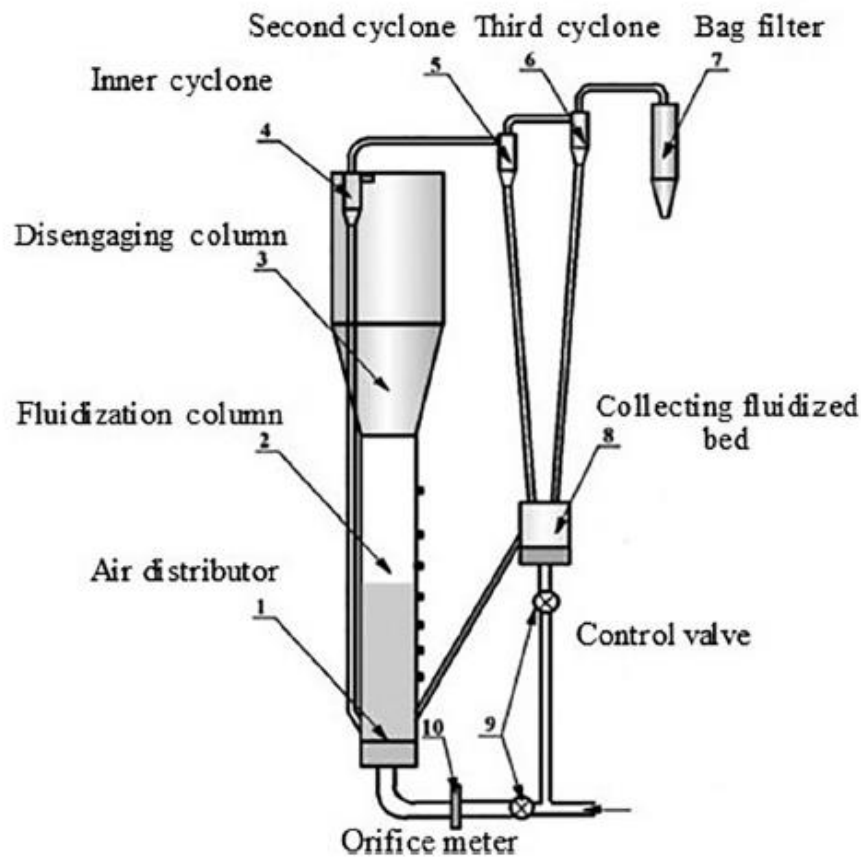


Figure 5.1 Simplified Diagram of Experimental Setup by Zhu et al. [2]

5.2 Simulation Setup

In this study, CFD modelling has been carried out of a bubbling fluidized bed comprising of Geldart A particles. Experimental work of Zhu et al. [2] has been used as reference for comparing with the simulation results. In previous studies related with TFM simulations by Li et al. [37], it has been concluded that two dimensional (2D) as well as three dimensional (3D) simulations can reproduce the hydrodynamical flows of a bubbling fluidized bed, thus in this simulation, 2D domain has been used to reduce the computational resources. 2D layout of the bubbling fluidized bed is shown in Fig. 5.2. All the grids are generated in Gambit ®2.4.6.

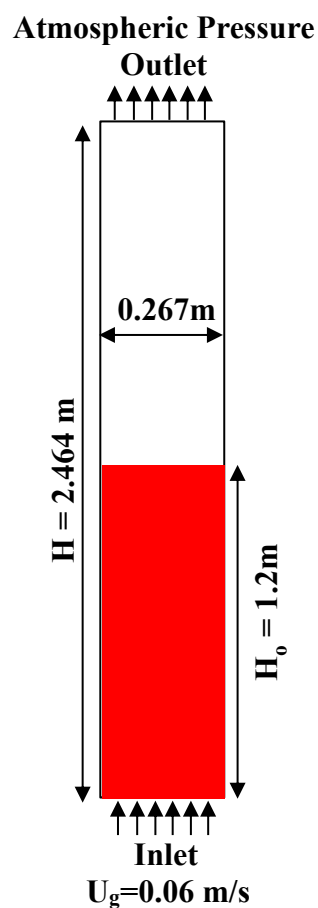


Figure 5.2: 2D layout of bubbling fluidized bed Zhu et al.[2]

Properties of solid particles comprising the bed and fluidizing medium (air) are given in Table 5.1.

Table 5.1: Solid Particles and Fluidizing Gas Properties [33]
Bed Material Properties

Parameter	Value
Particle density, kg/m ³	1780
Particle diameter, m	5.18 x 10 ⁻⁵
Mass of Particles, kg	319
Particle shape	Spherical
Air density, kg/m ³	1.225
Air viscosity, kg/ms	1.7894 x 10 ⁻⁵

There are two methods for particles patching in DDPM approach. One is surface injection and second is file injection [78]. In this study, solid particles have been patched using surface injection from the bottom surface of the column. Based upon the experimental data, the total mass of the particles patched is 319 kg. Solid particles are patched during the first one second of the simulation. Information required for surface injection is diameter of the particles, start and stop time, velocity and flow rate of the particles. After patching of the solid particles, bed is fluidized with the help of air entering from the bottom inlet.

5.2.1 Boundary and Initial Conditions

Air at the bottom inlet has a superficial velocity of 0.06 m/s. The gas phase is subject to a no-slip boundary condition on the walls, while the solid phase has a partial-slip boundary condition with a specular coefficient of 0.6. The pressure outlet boundary condition at the column outlet is set to atmospheric pressure, which is 101,325 Pa. In addition to using the specular coefficient for the walls in the DDPM, it is necessary to specify an extra, discrete phase boundary condition. ANSYS FLUENT ® 2021R1 offers various distinct phase boundary conditions for the wall boundary, including reflect, escape, trap, etc. In this study, we opted for the reflect boundary condition for the walls. This boundary condition accounts for the possibility of particles colliding with the wall and being reflected, either through elastic or inelastic collisions. In order to define the reflect boundary condition at the walls, it is necessary to have both a normal and tangential coefficient of restitution.

[15, 26].

Summary of boundary conditions is given in Table 5.2 [26].

Table 5.2: Summary of Boundary Conditions

Boundary	Value	Unit
Velocity Inlet	0.06	m/s
Pressure Outlet	101325	Pa
Walls	Gas phase = No slip	
	Solid phase = partial slip (0.6)	
	$e_{pw-normal} = 0.9$	
	$e_{pw-tangential} = 0.9$	

Summary of initial conditions is given in Table 5.3 [26].

Table 5.3: Summary of Initial Conditions

Initial Condition	Value	Unit
Height of Bed	1.2	m
Solid Volume Fraction	0.56	
Corresponding Mass of Solids	319	kg

The CFD simulations are conducted using the ANSYS FLUENT ® 2021R1 solver. The solver settings utilized are summarized in Table 5.4.

Table 5.4: Summary of Solver Settings

Unsteady state formulation	First order implicit
Pressure-velocity coupling	Phase-coupled-simple
Spatial discretization	Green-Gauss node-based
Momentum discretization	Second-order upwind
Volume fraction discretization	QUICK
Number of continuous iterations/ DPM	100
Restitution coefficient	0.6
Specularity coefficient	0.9
Maximum packing limit	0.63
Transition factor	1
Maximum number of iterations	50
Fluid time-step size	0.0005
Total simulation time	21 s

The simulations were conducted with a computational time step of 0.0005 seconds, spanning a total duration of 21 seconds. Once the initial 10 seconds have passed, data sampling is performed to gather time-based statistics. This is done since the residuals have reached a somewhat steady state by that point.

5.3 Grid Independence Test

Grid Independence Test in CFD (Computational Fluid Dynamics) is a technique used to ensure that the numerical solution obtained from a CFD simulation is independent of the grid or mesh resolution used. It is an important phase in the CFD modelling process since it aids in figuring out the ideal mesh size that yields precise results without using an excessive amount of computational resources. In this study, three square mesh sizes of 4 x 4 mm (corresponding to 77 x dp and 41272 mesh cells), 5 x 5 mm (corresponding to 96 x dp and 26076 mesh cells) and 7 x 7 mm (corresponding to 135 x dp and 13376 mesh cells) were evaluated. The simulations were conducted using the DDPM method, which was combined with the Wen-Yu drag model. All the three Meshes has been generated in Gambit @2.4.6. Fig. 5.3 shows the meshes generated for this simulation work.

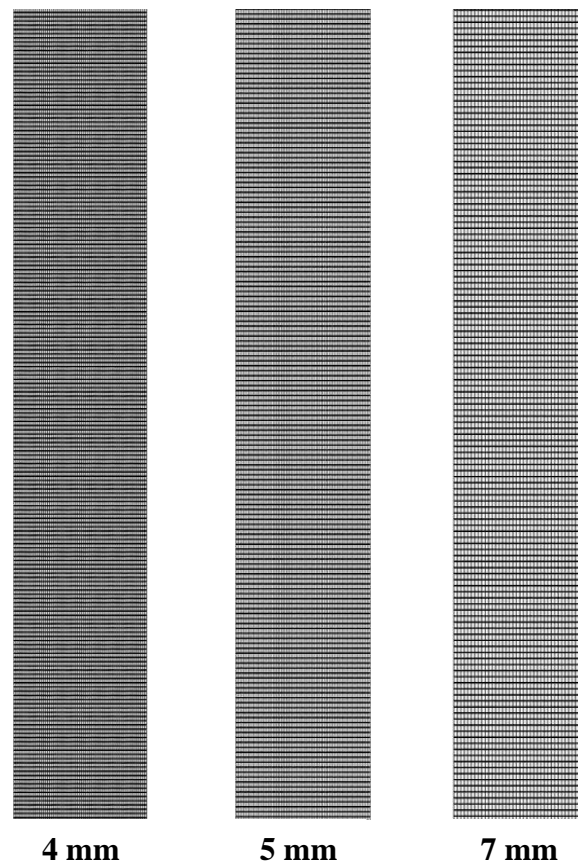


Figure 5.3: Different Mesh Size used for Grid Independence Test

Fig.5.4 displays instantaneous snapshots of the solid volume fraction distributions predicted using the Wen-Yu drag model for all three grid sizes. By observing the contours of the solid volume fraction at a given moment, it is evident that the Wen-Yu drag model can accurately depict the more subtle flow patterns when smaller grid sizes are used. Moreover, when the grid size increases, predicted bed height also increases.

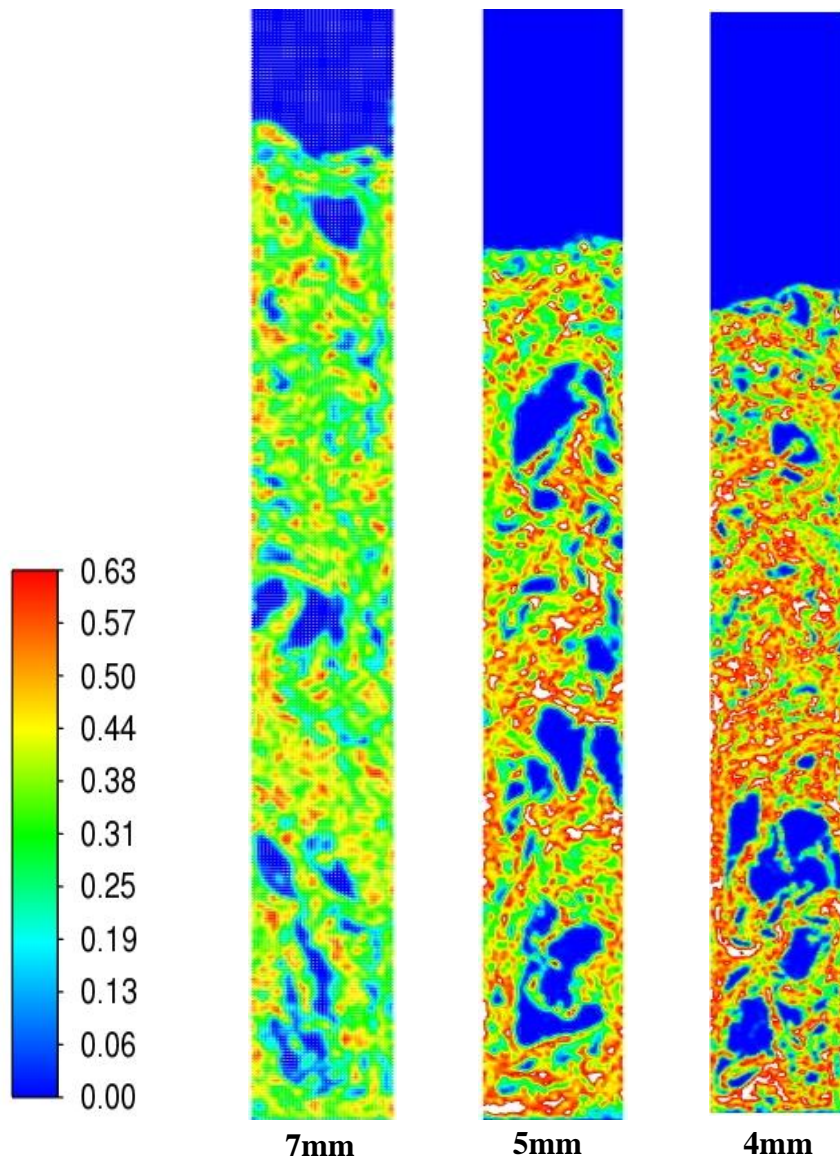


Figure 5.4: Instantaneous Solid Volume Fraction Contours

Fig. 5.5 (a) displays the time-averaged solids concentration contours for three different grid resolutions and Fig. 5.4 (b) illustrates the axial solid volume fraction. Upon evaluating the simulation findings, it has been revealed that the outcomes achieved with grid resolutions of 4 x 4 mm and 5 x 5 mm were more closely aligned with the experimental data and exhibited similarity when compared to the results produced with a grid size of 7 x 7 mm.

Therefore, grid size of 5 x 5 mm was selected for the remaining parts of the study for carrying out the simulations. This decision has been based on the consideration that using a 5 x 5 mm grid provided comparable results with 4 x 4 mm mesh size while requiring less computational time and cost, hence, making it a more favorable choice for the continuation of the research.

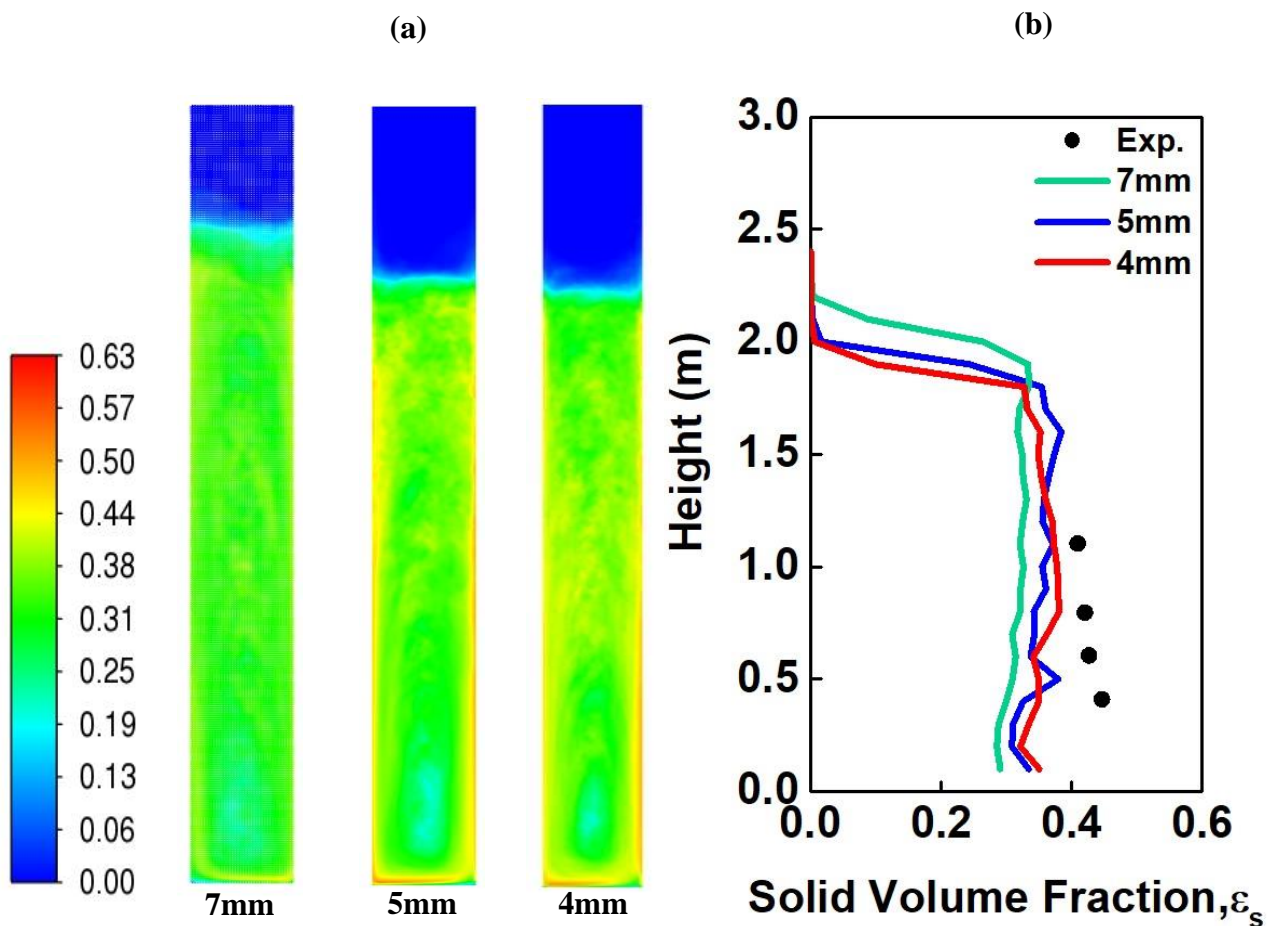


Figure 5.5: (a) Time Averaged Solid Volume Fraction (b) Axial Profile of Solid Volume Fraction

5.4 Comparison between Gidaspow and Wen – Yu Drag model

In vertical fluidized beds, drag force is overestimated in case of homogenous drag models because they fail to take into consideration the impacts of bubbles and clusters that arise from interactions between solid and gas particles and cohesive interparticle forces. In order to select the best homogeneous drag among between Gidaspow drag model and Wen – Yu drag model for further modification based on correction factor method, comparison based on instantaneous solid volume fraction contours, time averaged axial profiles, time averaged radial profiles and root mean square error is carried out as under.

5.4.1 Instantaneous Solid Volume Fraction Contours

Fig. 5.6 displays the distribution of solid volume fraction at a specific moment using the Gidaspow and Wen – Yu drag models. Based on the contour, it is clear that both drag models forecast the presence of bigger and more irregularly shaped bubbles. This is because these models are developed under the assumption of homogeneous gas-solid systems and do not take into account the existence of mesoscale heterogeneous structures and interparticle forces.

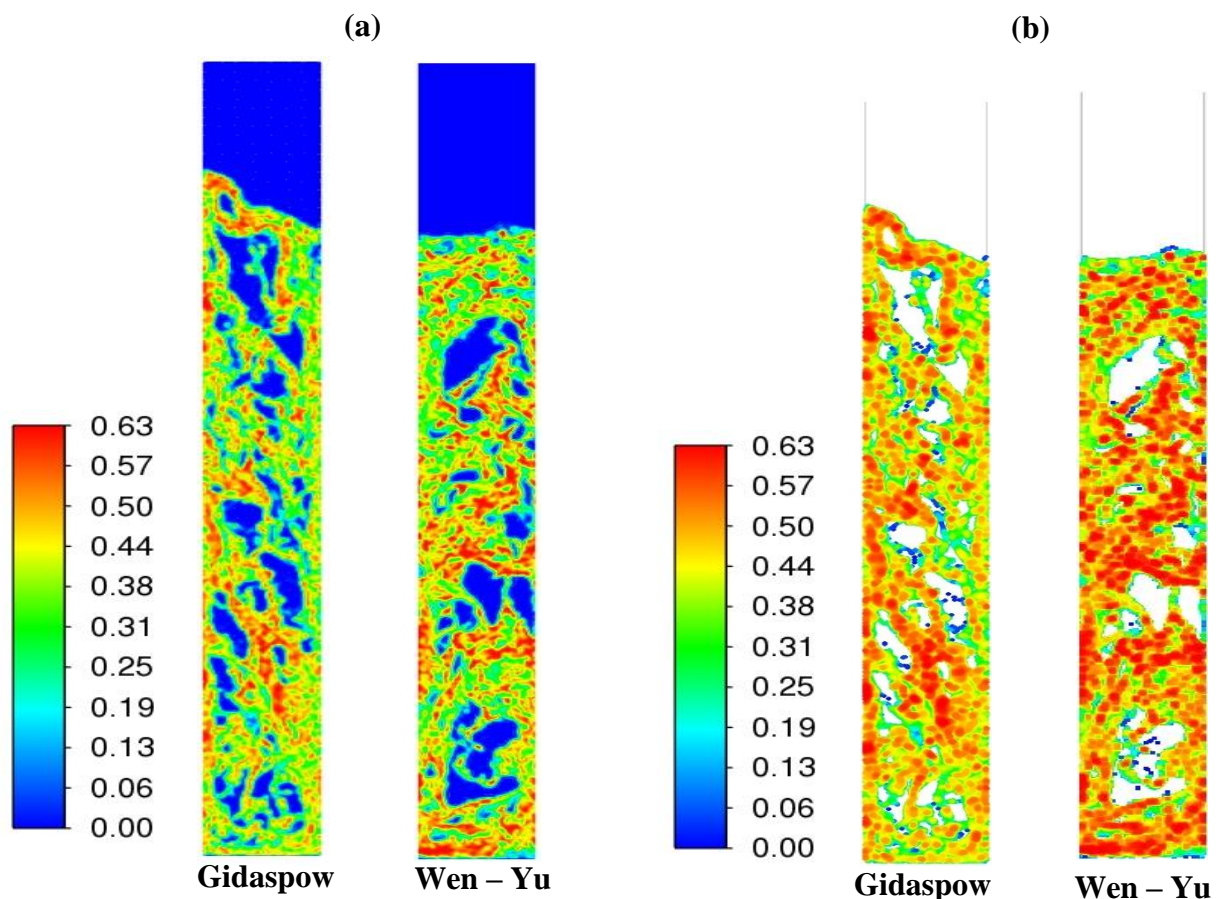


Figure 5.6: (a) Instantaneous Solid Volume Fraction Contour (b) Discrete Solid Volume Fraction contours

5.4.2 Time Averaged Axial Profile of Solid Volume Fraction

Fig. 5.7 displays the profiles of the solid volume fraction averaged over time, as predicted by the Gidaspow and Wen-Yu drag models. The axial profiles of solid volume fraction indicate that both the Gidaspow drag model and the Wen-Yu drag model follow the pattern found in a typical bubbling fluidized bed. This includes a high solid volume fraction at the lower end of the bed and a low solid volume fraction in the upper freeboard region. However, as compared to the experimental results, both drag models are forecasting a smaller solid volume fraction and a higher bed height.

These findings offer more proof that the drag force is overestimated in these models. The homogeneous drag models, which are derived from pressure drop tests using fixed or fluidized beds, are based on uniform gas solid systems, which explains the difference between the numerical simulations and the experimental results. Therefore, homogeneous drag models (such as Wen-Yu and Gidaspow) overestimate the drag force for heterogeneous gas-solid flow systems comprising of fine particles like Geldart A powders. Further, it can be seen from axial solid concentration profile that Wen –Yu model can predict better results of gas solid hydrodynamics than Gidaspow model for this particular case.

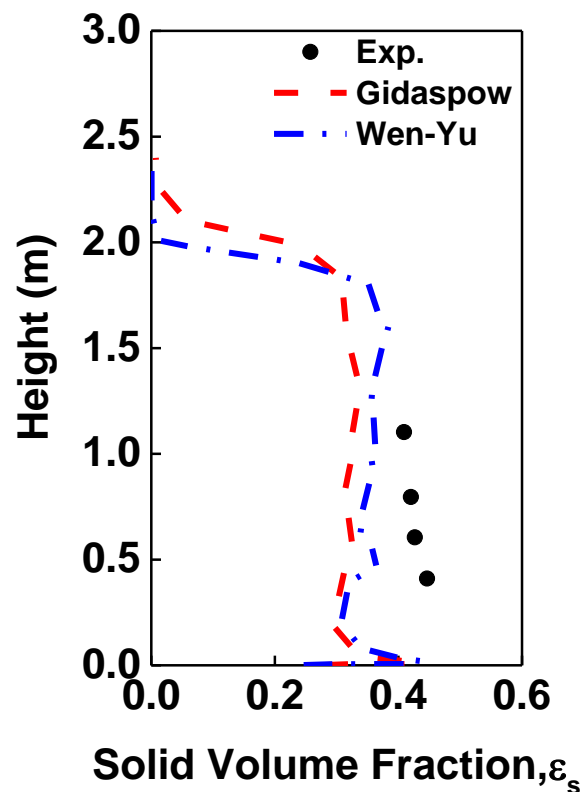


Figure 5.7: Time Averaged Axial Solid Volume Fraction

To find best drag model among the Gidaspow and Wen – Yu drag model, qualitative comparison based on root mean square error (RMSE) in predicted axial solids concentration has been carried out. Expression for the RMSE (-) is as under:-

$$RMSE = \sqrt{\frac{1}{n} \sum_{i=1}^n (\varepsilon_s^{experiment} - \varepsilon_s^{simulation})^2} \quad (26)$$

Here, n is the number of sample points, $\varepsilon_s^{experiment}$ is the solids concentration found from experiments and $\varepsilon_s^{simulation}$ is the value of solid concentration obtained from simulation results using Gidaspow and Wen – Yu drag model. A lower RMSE number implies that the simulation findings are more accurate and closely match the actual data, whereas a higher value indicates a greater deviation between the simulation and experimental results.

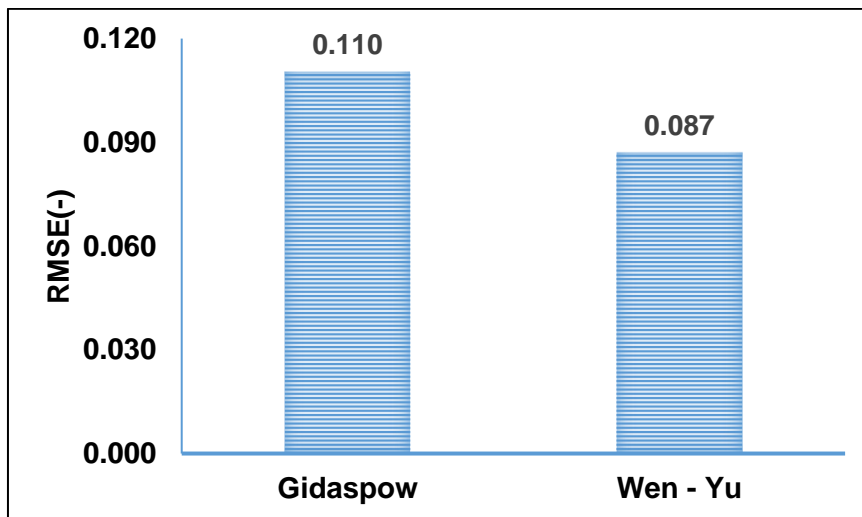


Figure 5.8: RMSE in Axial Solid Volume Fraction

It is evident from Fig.5.8 that RMSE value for axial solid volume fraction is smaller for Wen – Yu drag model compared to Gidaspow drag model. RMSE value for Gidaspow model is 20% more compared to Wen – Yu model.

5.4.3 Time Averaged Radial Profile of Solid Volume Fraction

Fig. 5.9 shows the time averaged radial solid volume fraction profiles at four different heights ($h=0.4$ m, $h=0.6$ m, $h=0.8$ m and $h=1.1$ m) predicted using the Gidaspow and Wen – Yu drag models. Simulation results has been compared with experimental data. The radial profiles indicate that both the Gidaspow drag model and the Wen-Yu drag model consistently underestimate the solid volume fraction relative to the experimental results at all four heights. These results confirm that both the Wen-Yu and Gidaspow drag models overestimate the drag force.

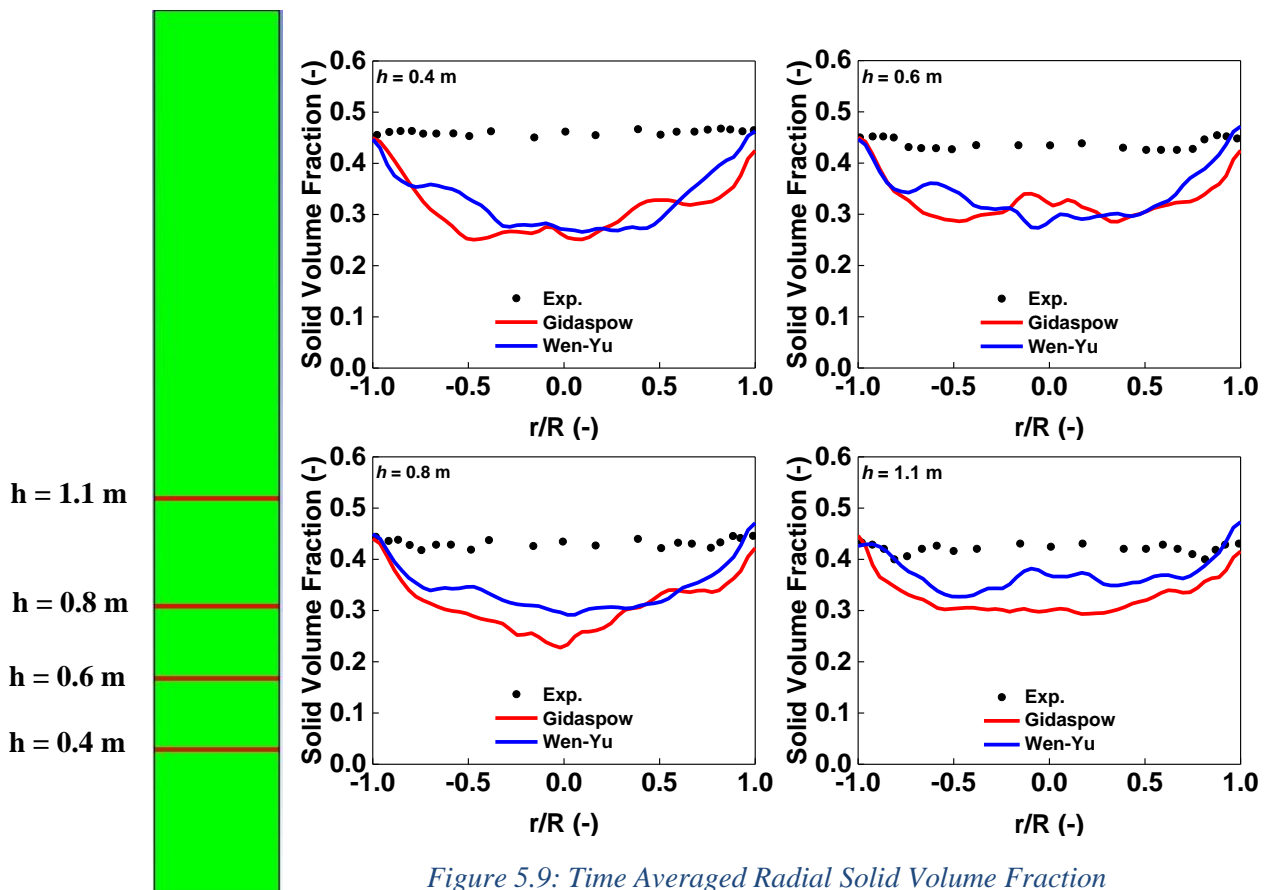


Figure 5.9: Time Averaged Radial Solid Volume Fraction

To find best drag model among the Gidaspow and Wen – Yu drag model, qualitative comparison based on root mean square error (RMSE) in predicting the radial solids concentration has been carried out. Expression for the RMSE (-) is as under:-

$$RMSE = \sqrt{\frac{1}{n} \sum_{i=1}^n (\epsilon_s^{experiment} - \epsilon_s^{simulation})^2} \quad (26)$$

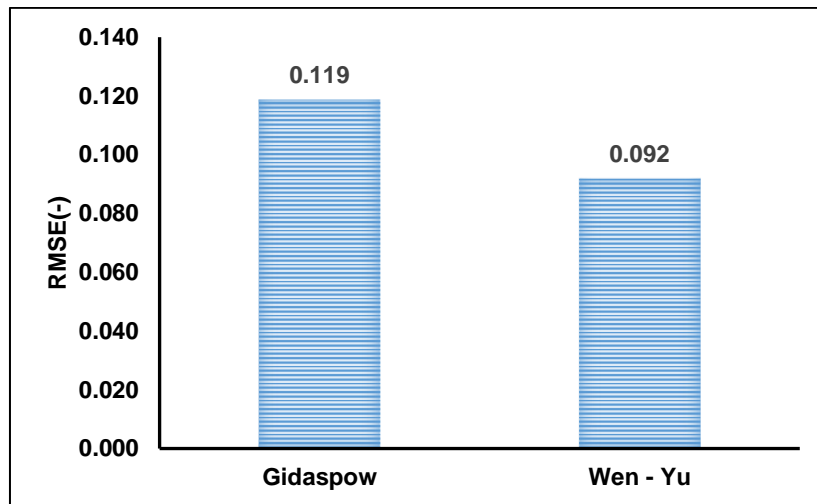


Figure 5.10 RMSE in Radial Solid Volume Fraction

It is evident from Fig.5.10 that RMSE value for radial solid volume fraction is smaller for Wen – Yu drag model compared to Gidaspow drag model. RMSE value for Gidaspow model is 22% more compared to Wen – Yu model.

From above discussion it can be concluded that Wen –Yu model can predict better results of gas solid hydrodynamics than Gidaspow model in this case of bubbling fluidized bed.

5.4.4 Time Averaged Solid Particles Velocity Vector Plot

Velocity of Solid particles in axial direction has been represented with the help of vector plots predicted by Gidaspow and Wen – Yu drag models in Fig 5.11 (a) & Fig 5.11 (b) respectively. The legend shows that red colour is a high velocity region whereas blue region within the bed is low / negative velocity region. It is evident from Fig 5.11 (a) that solids have higher velocity at the left wall and lower velocity at the right wall. Similarly the vector plots predicted by Wen – Yu drag model in Fig 5.11 (b) shows that solids have high velocity near right wall of column and low velocity near the left wall of the column. This trend of solids velocity is opposite to the experimental observations [26]. From experimental work, it is known that solid particles in bubbling fluidized bed, move in upward direction in the center of the column due to high velocity and fall back near the walls due to lower velocity. In this way, they make a core annulus pattern, in which solids move upward in the center region and fall back along the walls of the column.

It can be observed that both conventional drag models have failed to predict the core annulus pattern of solid particles flow within a bubbling fluidized bed. This result further confirms that homogeneous drag models cannot predict the hydrodynamics of Geldart A particles correctly.

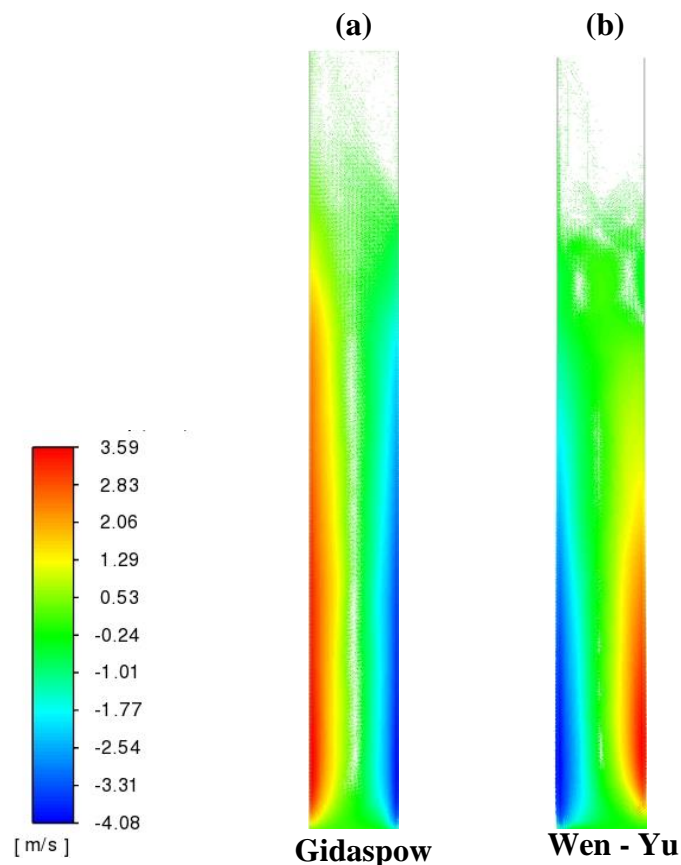


Figure 5.11: Solid Particles Velocity Vector Plot

5.5 Drag Modification and Drag Scale Factor

We have seen in the previous section that both the homogeneous drag models (Gidaspow and Wen – Yu) have failed to predict the solid volume fractions correctly and over predict the solid bed height because of over estimation of drag force which in turn is associated with the cohesive inter-particle forces, and mesoscale structures (bubbles) which are not accounted for in the derivation of homogeneous drag models. Most CFD models only take into account the inter-particle force resulting from particle-particle collisions [59, 93]. It has been reported in literature that cohesive inter-particle forces are significant for fine particles [53, 54]. Interparticle forces result in agglomeration of fine particles and in this way cause the fluid drag force to decrease.

Accurately simulating the cohesive forces that are crucial for fine particles is a challenging task, requiring realistic equations to represent them effectively. Ideally, modelling these inter-particle forces would enable the prediction of particle agglomeration and its impact on drag force. However, the calculation of van der Waals forces, in particular, is currently quite approximate.

In this section, a method has been devised to rectify the problem of over-prediction of drag force in numerical simulations by homogeneous drag models. The study looks at a scale factor / correction factor approach that McKeen and Pugsley first proposed [57]. In order to adequately predict the hydrodynamics of a bubbling fluidized bed of FCC particles, McKeen and Pugsley modified the Gibilaro's drag law by inserting an empirical correction factor varying between 0.2 and 0.3 in their investigation [57, 88]. They applied this method in numerical simulations related to the cold flow FCC stripper and the de-aeration of FCC fluidized beds. By multiplying the correction factor with original drag force coefficient, it is reduced by a certain percentage. In this way, drag force predicted by homogeneous drag model is reduced by a certain scale factor.

In present study, a correction factor known as “scale factor” has been used to modify the standard Wen – Yu drag model (which has predicted better results compared to Gidaspow Model). As a result of this modification, fluid particle drag reduces and thus it accounts for the cohesive interparticle forces and subscale level heterogeneous structures. In scale factor method, the standard drag coefficient is multiplied with dimensionless number (correction factor) to derive the modified drag coefficient. For this work, code has been written in C++ and then integrated with DDPM model with the help of user defined function.

- **Effect of Scale Factor on Solid Volume Fraction**

When the scale factor is set less than 1, it means drag force due to fluidizing gas will be lower than the standard drag force and solid particles will be less dispersed hence higher will be the solid volume fraction compared to the value predicted by the standard drag model. Conversely, a higher scale factor results in increasing the drag force, resulting in more dispersion of solid particles and decrease in solid volume fraction at the lower bed section compared to value predicted by standard drag model.

- **Effect of Scale Factor on Bed Expansion**

When the value of scale factor is set less than 1, it means drag force on the solid particles will be less, solid particles will not move farther away and will stay in lower section of the bed this in turn reduce the bed height compared the height predicted by the standard drag force. Similarly if the value of scale factor is greater than 1, it means drag force on solid particles will be more than the standard drag force, particles will move farther away and bed height will be more compared to the value predicted by standard drag force.

5.6 Modification of Wen – Yu Drag Model

In this section, we systematically applied different scale factors (0.3, 0.35, 0.4, 0.5, and 0.6) for the modification of Wen – Yu drag model for simulations of bubbling fluidized bed. Primary emphasis was on comprehending how these scale factors impact the expansion of the fluidized bed and the solid volume fraction, alongside comparing the simulation results with experimental data.

Simulation results has demonstrated a consistent trend that as the value of correction factor decreases, drag force decrease as a result of which the bed expansion height decreases while the solid volume fraction increased. This phenomenon can be linked with the above discussion related with scale factor.

5.6.1 Instantaneous Solids Concentration Contours

Fig. 5.12 (a) shows the instantaneous continuous solid concentration contours and Fig. 5.12 (b) shows the discrete solid concentration contours obtained from the simulation results by using correction factors (C) 0.3, 0.35, 0.4, 0.5 and 0.6. It is evident from the solid concentration contours that as the value of C increases, the bed height increases and size of the bubbles also increases. This is due to the reason that with increase in the value of C, the behavior of the drag model shifts towards the homogenous nature and the value of drag force increase which cause the bed height to increase.

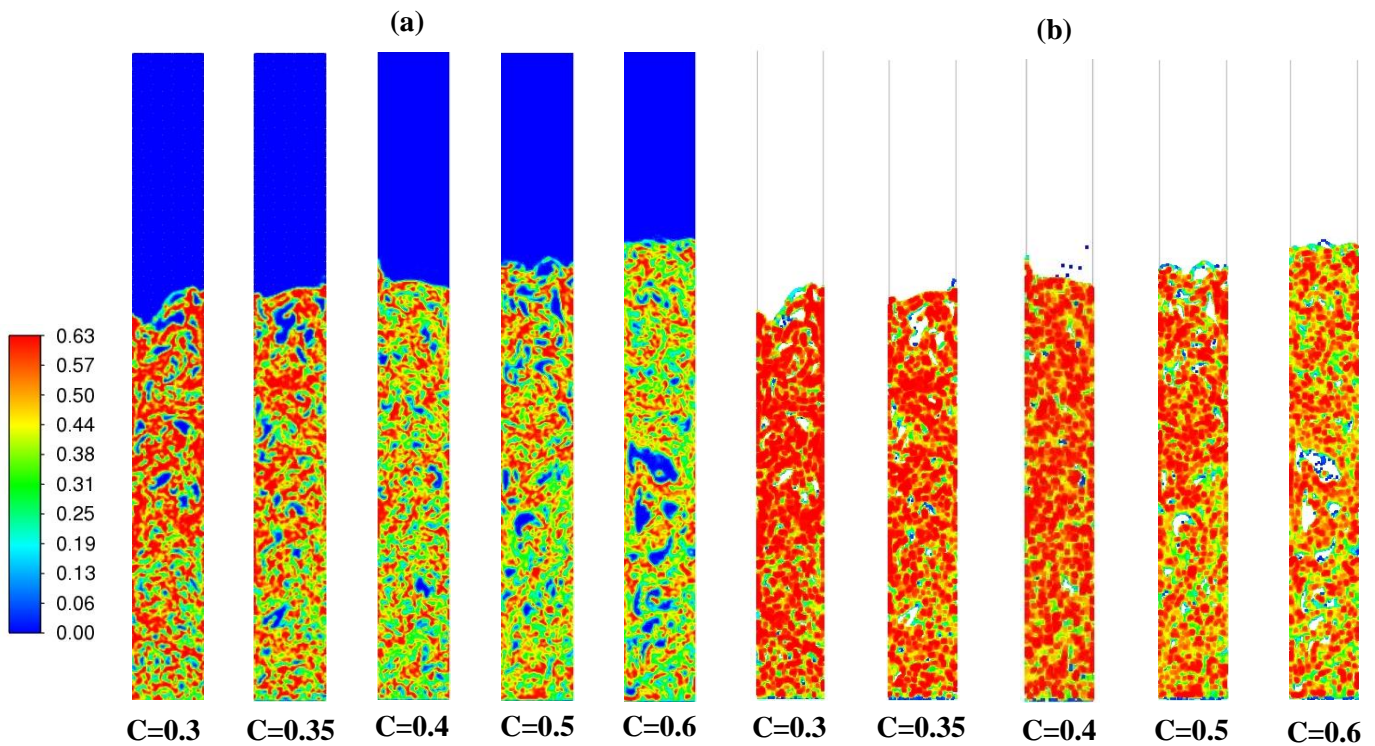


Figure 5.12: (a) Instantaneous Solid Volume Fraction Contours with Correction Factor (C) of 0.3, 0.35, 0.4, 0.5 and 0.6. (b) Discrete Solid Volume Fraction Contours with Correction Factor (C) of 0.3, 0.35, 0.4, 0.5 and 0.6

5.6.2 Time Averaged Axial Profile of Solid Volume Fraction

Fig. 5.13 shows the solid concentration profiles along the height of the bed (called as axial profile) obtained from the simulation results by using correction factors (C) 0.3, 0.35, 0.4, 0.5 and 0.6 for Wen – Yu drag model. When the value of correction factor (C) is set equal to 0.3 then the drag model predicts the higher solid concentration in the dense lower region of the bed compared to the experimental values because the drag value decrease at lower C values which cause the solid particles to remain at the lower portion of the bed. As the value of C increases from 0.3 to 0.6, axial solid concentration kept on decreasing and its lowest at 0.6 among all the tested C values. This is due to the reason that as the value of C increase, drag force increase which pushes the solid bed upwards, this causes a decrease in the solids concentration at the lower region of bed and increases the height of the bed.

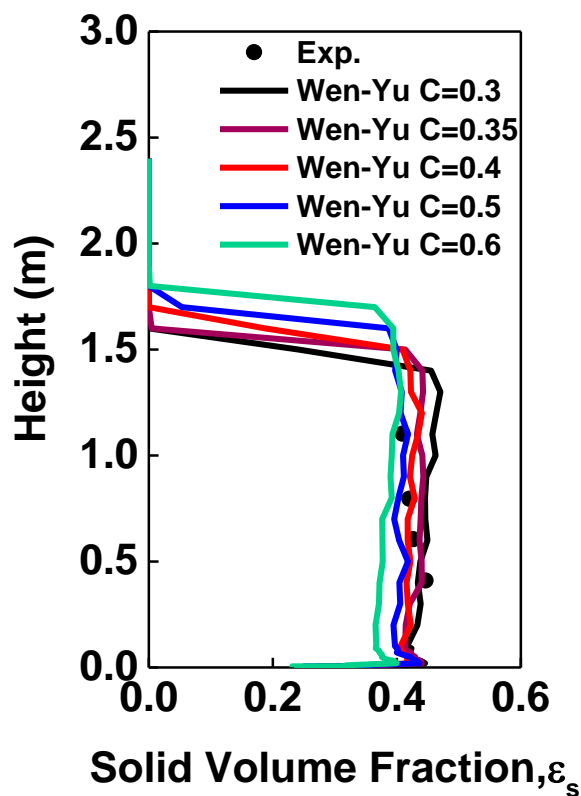


Figure 5.13: Axial Profile of Solid Volume Fraction with different Scale Factors

To find the most suitable value of correction factor (C) for finding the axial solids concentration, root mean square error (RMSE) has been calculated for each of the tested case. Expression for the RMSE (-) is as under:-

$$RMSE = \sqrt{\frac{1}{n} \sum_{i=1}^n (\varepsilon_s^{experiment} - \varepsilon_s^{simulation})^2} \quad (26)$$

Here, n is the number of sample points, $\varepsilon_s^{experiment}$ is the solids concentration found from experiments and $\varepsilon_s^{simulation}$ is the value of solid concentration obtained from simulation results using correction factor (0.3, 0.35, 0.4, 0.5, and 0.6). A lower RMSE number implies that the simulation findings are more accurate and closely match the actual data, whereas a higher value indicates a greater deviation between the simulation and experimental results.

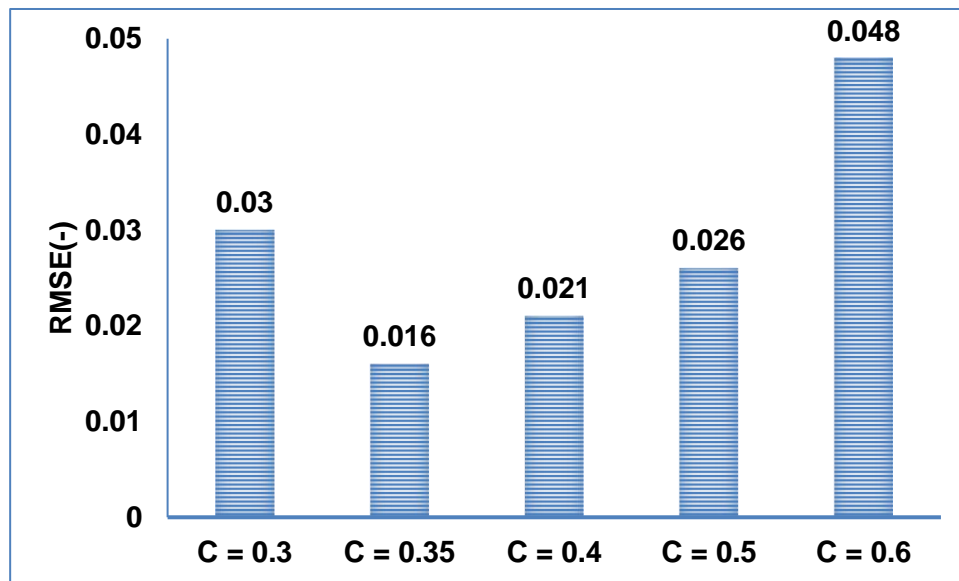


Figure 5.14: RMSE in Axial Solid Volume Fraction

It is evident from Fig.5.14 that RMSE value is smallest for correction factor of 0.35 and largest value of RMSE is for scale factor 0.6. These simulation results highlight the importance of selecting an appropriate correction factor when employing the Wen – Yu drag model in fluidized bed simulations. The choice of scale factor has a major impact on both bed expansion, solid volume fraction and radial volume fraction, which are critical parameters for accurately modelling fluidized bed systems. A scale factor of 0.35 has come out as a best choice in achieving accurate simulations that closely match experimental results.

5.6.3 Time Averaged Radial Profile of Solid Volume Fraction

Fig 5.15 compares the time average radial solid concentration with the experimental data at four different heights of the bed ($h=0.4$ m, $h=0.6$ m, $h=0.8$ m, $h=1.1$ m). Radial concentration profiles has been obtained using different correction factors ranging from $C=0.3$ to $C=0.6$. It is evident from the results that all the scale factors predict solid concentrations that follow the general rule of higher solid concentration near the walls and lower in the central region. At all the given heights, best match with experimental data is given by scale factor $C=0.35$ and lowest solid concentration is predicted by $C=0.6$.

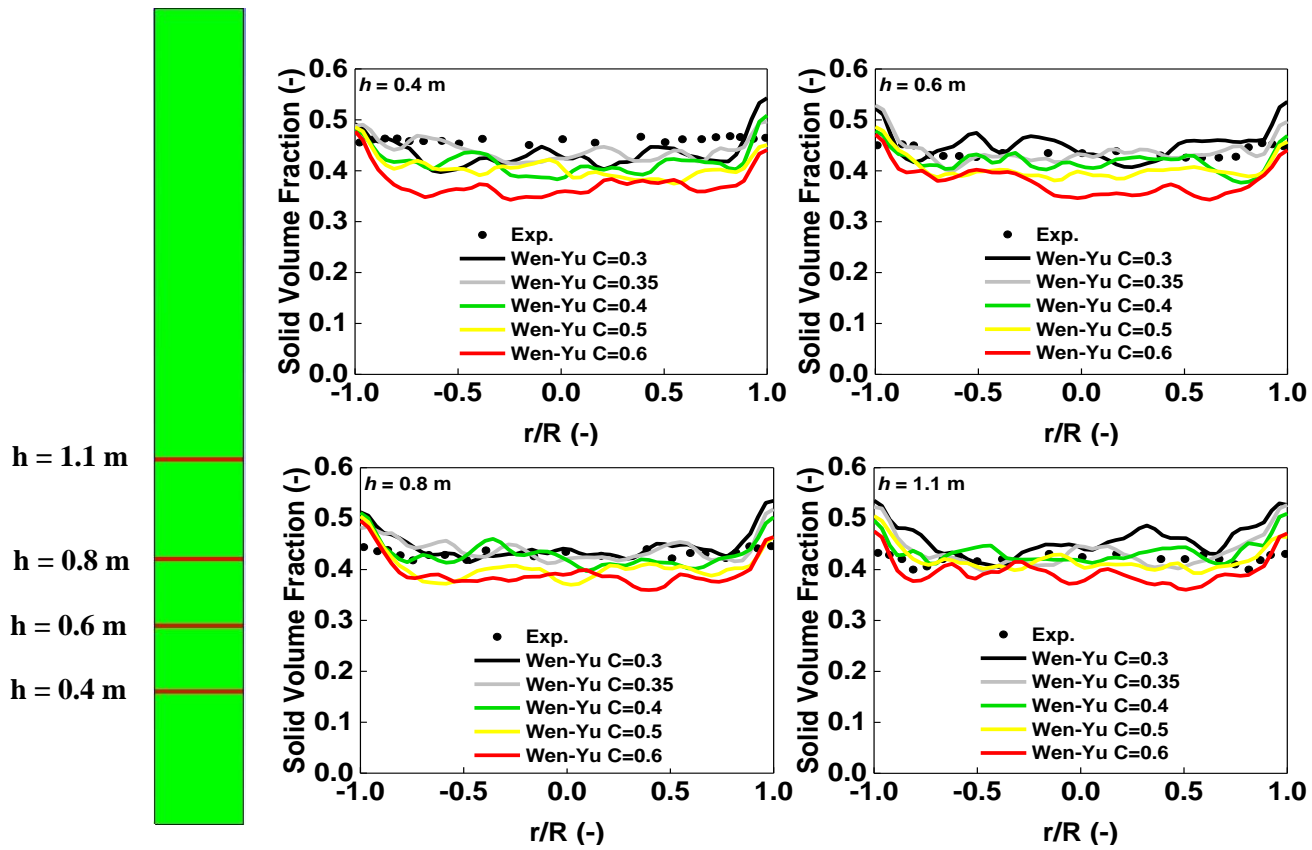


Figure 5.15: Time Averaged Radial Solid Volume Fraction with different Scale Factors

To find the most suitable value of correction factor (C) for finding the radial solids concentration, root mean square error (RMSE) has been calculated for each of the tested case. Expression for the RMSE (-) is as under:-

$$RMSE = \sqrt{\frac{1}{n} \sum_{i=1}^n (\varepsilon_s^{experiment} - \varepsilon_s^{simulation})^2} \quad (26)$$

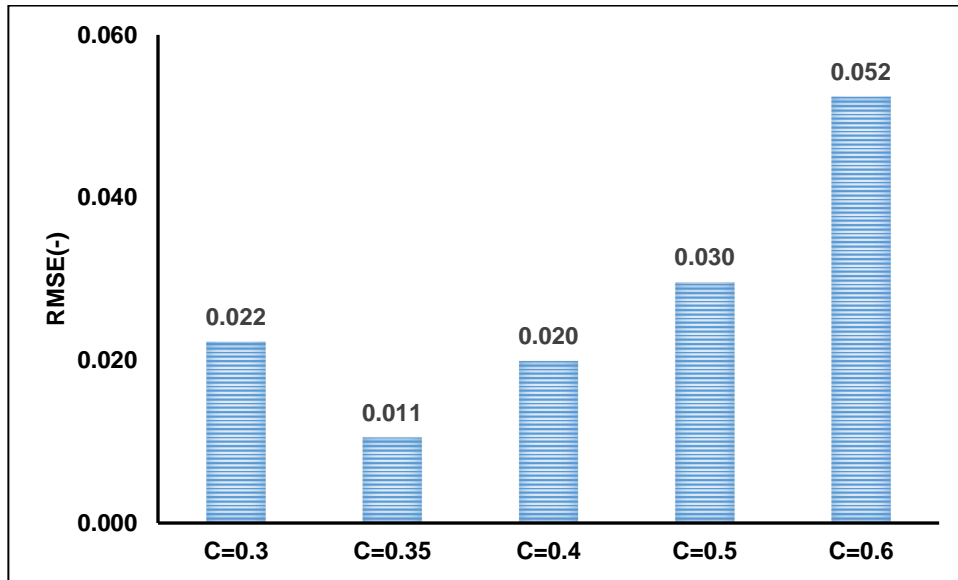


Figure 5.16 RMSE Value in Radial Solid Volume Fraction

It is evident from Fig.5.16 that RMSE value is smallest for correction factor of 0.35 and largest value of RMSE is for scale factor 0.6. These simulation results highlight the importance of selecting an appropriate correction factor when employing the Wen – Yu drag model in fluidized bed simulations. The choice of scale factor has a major impact on both bed expansion, solid volume fraction and radial volume fraction, which are critical parameters for accurately modelling fluidized bed systems. A scale factor of 0.35 has come out as a best choice in achieving accurate simulations that closely match experimental results.

5.6.1 Time Averaged Solid Particles Velocity Vector Plot

Fig.5.17 compares the velocity vector plots of solid particles predicted by Gidaspow, Wen – Yu and corrected Wen-Y drag models. In this snapshot, red colour shows the high velocity of the particles and blue colour shows the low velocity region. It is a characteristic of bubbling fluidized columns that solid particles move with high velocity in the central part and fall back along the walls of the column being the low velocity region. This pattern of solids flow is called as core annulus pattern. We can see that solid velocity vector plots in Fig 5.16 (a) and Fig 5.16 (b) which have been predicted by Gidaspow and Wen – Yu drag models do not follow the core annulus flow pattern. Whereas, the velocity vector plot predicted by corrected / modified Wen – Yu drag model in Fig. 5.16 (c) shows that solid particles are moving the central region and falling back along the walls thus following the core annulus flow pattern. This results further clarifies that for correct prediction of hydrodynamics of bubbling fluidized bed with Geldart A particles, it should be modified with a correction factor of $C=0.35$.

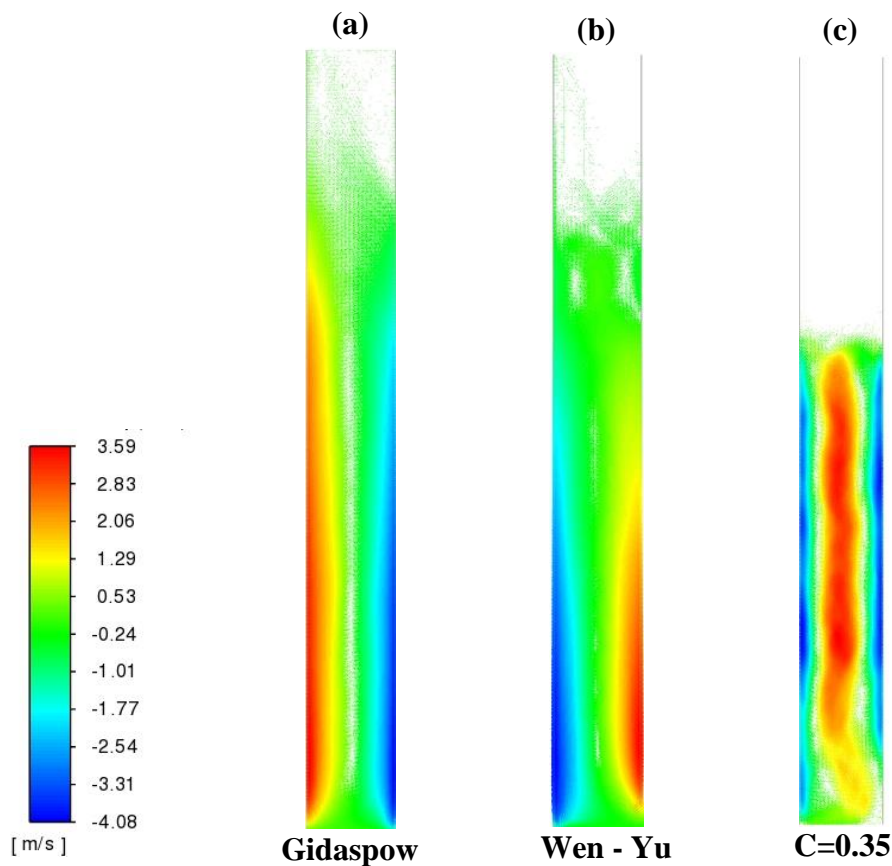


Figure 5.17: Solid Particles Velocity Vector Plot

CHAPTER 6: CONCLUSION AND RECOMMENDATION

In this research work, hydrodynamics of bubbling fluidized bed comprising of Geldart A particles has been studied using Dense Discrete Phase Modelling (DDPM) approach coupled with conventional Gidaspow drag model, conventional Wen – Yu drag model and modified Wen – Yu drag model. It has been observed that both conventional / homogeneous drag models integrated with DDPM approach cannot accurately predict the axial and radial solid volume fractions of Geldart A particles because these do not take into account the cohesive interparticle forces. However, solid volume fractions predicted by Wen – Yu drag model are closer to experimental data compared to the predictions made by Gidaspow drag model. Therefore, in this study Wen – Yu drag model was further corrected / modified by different correction factors (0.3, 0.35, 0.4, 0.5, and 0.6) to reduce its drag force and tested with DDPM model and it has been found that axial and radial solid volume fractions predicted with corrected Wen – Yu model with correction factor $C=0.35$ best match with the experimental results.

DDPM is a novel approach as compared to other CFD modelling approaches (DEM and TFM). This work is the first step for modification of the experimental Wen – Yu drag model using empirical approach and its implementation to study the hydrodynamics of low velocity gas – solid bubbling bed which has been done successfully.

It is recommended to implement the DDPM approach with empirical drag correction model for the high velocity turbulent and circulating regimes for further maturity of the model.

REFERENCES

- [1]. Zhou, Y., T. Wang, and J. Zhu, *Development of gas-solid fluidization: particulate and aggregative*. Powder Technology, 2023. **421**: p. 118420.
- [2]. Zhu, H., et al., *Detailed measurements of flow structure inside a dense gas–solids fluidized bed*. Powder Technology, 2008. **180**(3): p. 339-349.
- [3]. Li, T., S. Pannala, and M. Shahnab, *CFD simulations of circulating fluidized bed risers, part II, evaluation of differences between 2D and 3D simulations*. Powder technology, 2014. **254**: p. 115-124.
- [4]. Dubrawski, K., et al., *Traveling column for comparison of invasive and non-invasive fluidization voidage measurement techniques*. Powder technology, 2013. **235**: p. 203-220.
- [5]. Geldart, D., *Types of gas fluidization*. Powder technology, 1973. **7**(5): p. 285-292.
- [6]. Kunii, D. and O. Levenspiel, *Fluidization engineering*. 1991: Butterworth-Heinemann.
- [7]. Basu, P. and S.A. Fraser, *Circulating fluidized bed boilers*. 1991: Springer
- [8]. King, D., *Fluidized catalytic crackers: an engineering review*. Fluidization VII, 1992: p. 15-26.
- [9]. Keil, F.J., *Methanol-to-hydrocarbons: process technology*. Microporous and mesoporous materials, 1999. **29**(1-2): p. 49-66.
- [10]. Rashid, T.A.B., L.-T. Zhu, and Z.-H. Luo, *Comparative analysis of numerically derived drag models for development of bed expansion ratio correlation in a bubbling fluidized bed*. Advanced Powder Technology, 2020. **31**(7): p. 2723-2732.
- [11]. Agrawal, K., et al., *The role of meso-scale structures in rapid gas–solid flows*. Journal of Fluid Mechanics, 2001. **445**: p. 151-185.
- [12]. Dong, W., W. Wang, and J. Li, *A multiscale mass transfer model for gas–solid riser flows: Part I—Sub-grid model and simple tests*. Chemical Engineering Science, 2008. **63**(10): p. 2798-2810.
- [13]. Dong, W., W. Wang, and J. Li, *A multiscale mass transfer model for gas–solid riser flows: Part II—Sub-grid simulation of ozone decomposition*. Chemical Engineering Science, 2008. **63**(10): p. 2811-2823.
- [14]. Shehryar, A., et al., *Model for predicting solids velocity fluctuations in sedimenting suspensions*. Chemical Engineering & Technology, 2019. **42**(12): p. 2641-2648.
- [15]. Fluent, A., *14.5 User Guide, “ANSYS Inc., ”*. 2007, Springer Berlin Heidelberg, New York.
- [16]. Adamczyk, W.P., *Application of the numerical techniques for modelling fluidization process within industrial scale boilers*. Archives of Computational Methods in Engineering, 2017. **24**(4): p. 669-702.

- [17]. Ding, J. and D. Gidaspow, *A bubbling fluidization model using kinetic theory of granular flow*. AIChE journal, 1990. **36**(4): p. 523-538.
- [18]. Altantzis, C., R.B. Bates, and A.F. Ghoniem, *3D Eulerian modeling of thin rectangular gas–solid fluidized beds: estimation of the specular coefficient and its effects on bubbling dynamics and circulation times*. Powder Technology, 2015. **270**: p. 256-270.
- [19]. Asegehegn, T.W., M. Schreiber, and H.J. Krautz, *Influence of two-and three-dimensional simulations on bubble behavior in gas–solid fluidized beds with and without immersed horizontal tubes*. Powder Technology, 2012. **219**: p. 9-19.
- [20]. Bakshi, A., et al., *Eulerian–Eulerian simulation of dense solid–gas cylindrical fluidized beds: Impact of wall boundary condition and drag model on fluidization*. Powder Technology, 2015. **277**: p. 47-62.
- [21]. Ostermeier, P., et al., *Numerical calculation of wall-to-bed heat transfer coefficients in Geldart B bubbling fluidized beds with immersed horizontal tubes*. Powder technology, 2018. **333**: p. 193-208.
- [22]. Ostermeier, P., et al., *Three dimensional multi fluid modeling of Geldart B bubbling fluidized bed with complex inlet geometries*. Powder technology, 2017. **312**: p. 89-102.
- [23]. Diba, M.F., M.R. Karim, and J. Naser, *Fluidized bed CFD using simplified solid-phase coupling*. Powder Technology, 2020. **375**: p. 161-173.
- [24]. Ullah, A., et al., *Effect of turbulence modeling on hydrodynamics of a turbulent contact absorber*. Chemical Engineering and Processing-Process Intensification, 2020. **156**: p. 108101.
- [25]. Ahmad, N., et al., *Extending the EMMS-bubbling model to fluidization of binary particle mixture: Parameter analysis and model validation*. Chemical Engineering Science, 2019. **200**: p. 257-267.
- [26]. Adnan, M., et al., *Verification and validation of the DDPM-EMMS model for numerical simulations of bubbling, turbulent and circulating fluidized beds*. Powder technology, 2021. **379**: p. 69-88.
- [27]. Cundall, P.A., *A Discrete numerical model for granular assemblies Geotechnique*. Geotechnique, 1979. **29**: p. 47-65.
- [28]. Wu, Y., et al., *Numerical simulation of circulating fluidized bed oxy-fuel combustion with Dense Discrete Phase Model*. Fuel processing technology, 2019. **195**: p. 106129.
- [29]. Muhammad, A., N. Zhang, and W. Wang, *CFD simulations of a full-loop CFB reactor using coarse-grained Eulerian–Lagrangian dense discrete phase model: Effects of modeling parameters*. Powder technology, 2019. **354**: p. 615-629.
- [30]. Farid, M.M., et al., *Numerical investigation of particle transport hydrodynamics and coal combustion in an industrial-scale circulating fluidized bed combustor: Effects of coal feeder positions and coal feeding rates*. Fuel, 2017. **192**: p. 187-200.
- [31]. Andrews, M.J. and P.J. O'Rourke, *The multiphase particle-in-cell (MP-PIC) method for dense particulate flows*. International Journal of Multiphase Flow, 1996. **22**(2): p. 379-402.

- [32]. Kraft, S., F. Kirnbauer, and H. Hofbauer, *Influence of drag laws on pressure and bed material recirculation rate in a cold flow model of an 8 MW dual fluidized bed system by means of CPFD*. Particuology, 2018. **36**: p. 70-81
- [33]. Adnan, M., et al., *Comparative CFD modeling of a bubbling bed using a Eulerian–Eulerian two-fluid model (TFM) and a Eulerian-Lagrangian dense discrete phase model (DDPM)*. Powder Technology, 2021. **383**: p. 418-442.
- [34]. Chapman, S. and T.G. Cowling, *The mathematical theory of non-uniform gases: an account of the kinetic theory of viscosity, thermal conduction and diffusion in gases*. 1990: Cambridge university press.
- [35]. Feng, M., et al., *Parametric study for MP-PIC simulation of bubbling fluidized beds with Geldart A particles*. Powder technology, 2018. **328**: p. 215-226
- [36]. Wang, H. and Y. Lu, *Numerical simulation of bubble behavior in a quasi-2D fluidized bed using a bubble-based EMMS model*. Particuology, 2019. **46**: p. 40-54.
- [37]. Li, J. and B. Yang, *CFD simulation of bubbling fluidized beds using a local-structure-dependent drag model*. Chemical Engineering Journal, 2017. **329**: p. 100-115.
- [38]. Kshetrimayum, K.S., et al., *EMMS drag model for simulating a gas–solid fluidized bed of geldart B particles: Effect of bed model parameters and polydispersity*. Particuology, 2020. **51**: p. 142-154.
- [39]. Vejahati, F., et al., *CFD simulation of gas–solid bubbling fluidized bed: a new method for adjusting drag law*. The Canadian Journal of Chemical Engineering, 2009. **87**(1): p. 19-30.
- [40]. Wang, S., et al., *Modeling of bubble-structure-dependent drag for bubbling fluidized beds*. Industrial & Engineering Chemistry Research, 2014. **53**(40): p. 15776-15785.
- [41]. Shi, Z., W. Wang, and J. Li, *A bubble-based EMMS model for gas–solid bubbling fluidization*. Chemical Engineering Science, 2011. **66**(22): p. 5541-5555.
- [42]. Luo, H., et al., *A grid-independent EMMS/bubbling drag model for bubbling and turbulent fluidization*. Chemical Engineering Journal, 2017. **326**: p. 47-57.
- [43]. Hong, K., et al., *Extending the bubble-based EMMS model to CFB riser simulations*. Powder technology, 2014. **266**: p. 424-432.
- [44]. Cloete, S., S. Amini, and S.T. Johansen, *A fine resolution parametric study on the numerical simulation of gas–solid flows in a periodic riser section*. Powder Technology, 2011. **205**(1-3): p. 103-111
- [45]. Kumar, U. and V. Agarwal, *Simulation of 3D gas–solid fluidized bed reactor hydrodynamics*. Particulate Science and Technology, 2017. **35**(1): p. 1-13.
- [46]. Taghipour, F., N. Ellis, and C. Wong, *Experimental and computational study of gas–solid fluidized bed hydrodynamics*. Chemical engineering science, 2005. **60**(24): p. 6857-6867.
- [47]. Loha, C., H. Chattopadhyay, and P.K. Chatterjee, *Assessment of drag models in simulating bubbling fluidized bed hydrodynamics*. Chemical Engineering Science, 2012. **75**: p. 400-407.
- [48]. Parmentier, J.-F., O. Simonin, and O. Delsart, *A numerical study of fluidization behavior of Geldart B, A/B and A particles using an Eulerian multifluid modeling approach*. 2008.

- [49]. Lu, B., W. Wang, and J. Li, *Eulerian simulation of gas–solid flows with particles of Geldart groups A, B and D using EMMS-based meso-scale model*. Chemical Engineering Science, 2011. **66**(20): p. 4624-4635.
- [50]. Nikolopoulos, A., et al., *An advanced EMMS scheme for the prediction of drag coefficient under a 1.2 MWth CFBC isothermal flow—Part II: Numerical implementation*. Chemical Engineering Science, 2010. **65**(13): p. 4089-4099.
- [51]. Benyahia, S., *Fine-grid simulations of gas-solids flow in a circulating fluidized bed*. AIChE Journal, 2012. **58**(11).
- [52]. Van Wachem, B., et al., *Comparative analysis of CFD models of dense gas–solid systems*. AIChE Journal, 2001. **47**(5): p. 1035-1051.
- [53]. Grace, J. and G. Sun, *Influence of particle size distribution on the performance of fluidized bed reactors*. The Canadian Journal of Chemical Engineering, 1991. **69**(5): p. 1126-1134.
- [54]. Massimilla, L. and G. Donsì, *Cohesive forces between particles of fluid-bed catalysts*. Powder Technology, 1976. **15**(2): p. 253-260.
- [55]. POWDERS, O.F., *THE DYNAMICS OF FINE POWDERS*.
- [56]. Fan, L.-S. and C. Zhu, *Principles of gas-solid flows*. 1999.
- [57]. Mckeen, T. and T. Pugsley, *Simulation and experimental validation of a freely bubbling bed of FCC catalyst*. Powder Technology, 2003. **129**(1-3): p. 139-152.
- [58]. Davidson, J. and D. Harrison, *The behaviour of a continuously bubbling fluidised bed*. Chemical Engineering Science, 1966. **21**(9): p. 731-738.
- [59]. Geldart, D., *Gas fluidization technology*. 1986.
- [60]. Kwauk, M., *Particulate fluidization: an overview*. Advances in chemical engineering, 1991. **17**: p. 207-360.
- [61]. Zhu, J.X., et al., *(Gas-) liquid-solid circulating fluidized beds and their potential applications to bioreactor engineering*. The Canadian Journal of Chemical Engineering, 2000. **78**(1): p. 82-94.
- [62]. Wilhelm, R.H., *Fluidization of solid particles*. Chem. Eng. Prog., 1948. **44**: p. 201-218.
- [63]. Oke, O., et al., *Numerical simulations of lateral solid mixing in gas-fluidized beds*. Chemical Engineering Science, 2014. **120**: p. 117-129.
- [64]. Shen, L., M. Zhang, and Y. Xu, *Solids mixing in fluidized beds*. Powder technology, 1995. **84**(3): p. 207-212.
- [65]. Kunii, D. and O. Levenspiel, *Bubbling bed model. Model for flow of gas through a fluidized bed*. Industrial & Engineering Chemistry Fundamentals, 1968. **7**(3): p. 446-452.
- [66]. Chen, X. and J. Wang, *A comparison of two-fluid model, dense discrete particle model and CFD-DEM method for modeling impinging gas–solid flows*. Powder technology, 2014. **254**: p. 94-102.

- [67]. Zhang, Y., X. Lan, and J. Gao, *Modeling of gas-solid flow in a CFB riser based on computational particle fluid dynamics*. Petroleum Science, 2012. **9**: p. 535-543.
- [68]. Abbasi, A., et al., *CPFD flow pattern simulation in downer reactors*. AIChE Journal, 2013. **59**(5): p. 1635-1647.
- [69]. Abbasi, A., P.E. Ege, and H.I. De Lasa, *CPFD simulation of a fast fluidized bed steam coal gasifier feeding section*. Chemical Engineering Journal, 2011. **174**(1): p. 341-350.
- [70]. Chen, C., et al., *CPFD simulation of circulating fluidized bed risers*. Powder technology, 2013. **235**: p. 238-247.
- [71]. Yin, S., et al., *Modeling on the hydrodynamics of pressurized high-flux circulating fluidized beds (PHFCFBs) by Eulerian–Lagrangian approach*. Powder technology, 2014. **259**: p. 52-64.
- [72]. Lu, H., et al., *Experimental and CPFD numerical study on hopper discharge*. Industrial & Engineering Chemistry Research, 2014. **53**(30): p. 12160-12169.
- [73]. Li, T., et al., *Open-source MFIX-DEM software for gas-solids flows: Part II—Validation studies*. Powder Technology, 2012. **220**: p. 138-150.
- [74]. Cheng, Y., et al., *Downer reactor: from fundamental study to industrial application*. Powder Technology, 2008. **183**(3): p. 364-384.
- [75]. Garg, R., et al., *Open-source MFIX-DEM software for gas–solids flows: Part I—Verification studies*. Powder Technology, 2012. **220**: p. 122-137.
- [76]. Ariyaratne, W.H., et al. *CFD approaches for modeling gas-solids multiphase flows—A review*. in *9th EUROSIM & the 57th SIMS Conference, Oulu*. 2016.
- [77]. Michaelides, E.E., M. Sommerfeld, and B. van Wachem, *Multiphase flows with droplets and particles*. 2022: CRC Press.
- [78]. Adnan, M., et al., *Coarse-graining dense discrete phase model for modeling particle dynamics in a 3D tapered fluidized bed coater: Analysis of different drag models*. Journal of Food Engineering, 2024. **365**: p. 111831.
- [79]. Hashemisohe, A., et al., *Numerical analysis and experimental validation of hydrodynamics of a thin bubbling fluidized bed for various particle-size distributions using a three-dimensional dense discrete phase model*. Particuology, 2020. **49**: p. 191-204.
- [80]. Adamczyk, W.P., et al., *Modeling of particle transport and combustion phenomena in a large-scale circulating fluidized bed boiler using a hybrid Euler–Lagrange approach*. Particuology, 2014. **16**: p. 29-40.
- [81]. Gidaspow, D., R. Bezburuah, and J. Ding, *Hydrodynamics of circulating fluidized beds: kinetic theory approach*. 1991, Illinois Inst. of Tech., Chicago, IL (United States). Dept. of Chemical
- [82]. Schaeffer, D.G., *Instability in the evolution equations describing incompressible granular flow*. Journal of differential equations, 1987. **66**(1): p. 19-50.
- [83]. LUN, C., S. SAVAGE, and D. JEFFREY, *Kinetic theories for granular flow: inelastic*.

- [84]. Adnan, M., et al., *Multiscale modeling of bubbling fluidized bed reactors using a hybrid Eulerian-Lagrangian dense discrete phase approach*. Powder Technology, 2020. **376**: p. 296-319.
- [85]. Ergun, S., *Fluid flow through packed columns*. Chem. Eng. Prog., 1952. **48**(2): p. 89-94.
- [86]. Ergun, S., *Fluid flow through packed columns*. Chemical engineering progress, 1952. **48**(2): p. 89.
- [87]. Niven, R.K., *Physical insight into the Ergun and Wen & Yu equations for fluid flow in packed and fluidised beds*. Chemical Engineering Science, 2002. **57**(3): p. 527-534.
- [88]. Li, T., et al., *Numerical simulation of horizontal jet penetration in a three-dimensional fluidized bed*. Powder Technology, 2008. **184**(1): p. 89-99.